# New Approach to Tolman's Electronic Parameter Based on Local Vibrational Modes

Robert Kalescky, Elfi Kraka, and Dieter Cremer*

Department of Chemistry, Southern Methodist University, 3215 Daniel Avenue, Dallas, Texas 75275-0314, United States

Ⓢ *Supporting Information*

ABSTRACT: Tolman's electronic parameter (TEP) derived from the A_1-symmetrical CO stretching frequency of nickel–phosphine–tricarbonyl complexes, $R_3PNi(CO)_3$, is brought to a new, improved level by replacing normal with local vibrational frequencies. CO normal vibrational frequencies are always flawed by mode–mode coupling especially with metal–carbon stretching modes, which leads to coupling frequencies as large as 100 cm^{-1} and can become even larger when the transition metal and the number of ligands is changed. Local TEP (LTEP) values, being based on local CO stretching force constants rather than normal mode frequencies, no longer suffer from mode coupling and mass effects. For 42 nickel complexes of the type $LNi(CO)_3$, it is shown that LTEP values provide a different ordering of ligand electronic effects as previously suggested by TEP and CEP values. The general applicability of the LTEP concept is demonstrated.
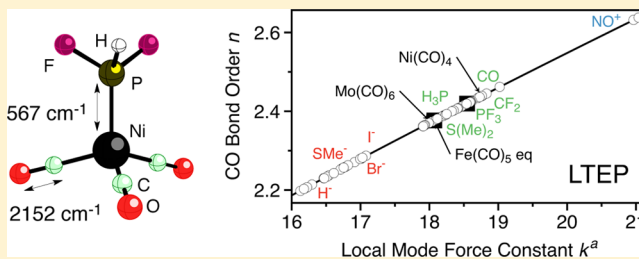
1. INTRODUCTION

An easy but basic understanding of the electronic influence of ligands in transition metal chemistry is one of the prerequisites for the design of suitable catalysts in homogeneous catalysis. Molecular orbital theory in combination with reliable quantum chemical calculations can provide valuable and detailed insight in this connection. However, an experimental measure for the ligand electronic and steric activity is an attractive alternative as it circumvents lengthy discussions about the accuracy of the method and/or basis set used in the quantum chemical calculations.

The Tolman electronic parameter (TEP) and the Tolman cone angle θ[1,2] represent such measures describing the electronic and steric properties of phosphine ligands in transition metal complexes. The TEP is derived from the A_1-symmetrical CO stretching frequency in the infrared spectrum spectrum of nickel–tricarbonyl–phosphine complexes of the type $R_3PNi(CO)_3$ because this vibrational frequency is well-separated from other frequencies and can easily be detected in the measured spectrum. Phosphine ligands possess a distinct electronic and steric tunability, seldom participate directly in the reactions of a transition metal complex, and can be used to modulate the electronic properties of the adjoint metal center.[3]

Phosphines[3] are σ-donors, where their donor ability increases (decreases) with R being an alkyl (aryl) group or any other electron-donating (withdrawing) substituent R. Electron-donating phosphines increase the electron density at the metal, and accordingly, the metal is more prone to back-bonding with the CO ligands, which involves a $d\pi(M)$-$\pi^\star(CO)$ interaction, which weakens the CO bond strength. The change in the CO bond strength is sensitively registered by the A_1-symmetrical CO stretching frequency, which therefore was chosen by Tolman as a measure for the electronic activity of the phosphine ligand. The TEP, as simple and useful as it is, faces two major complications. Phosphines can also be involved in back-donation via a $d\pi(M)$-$\sigma^\star(P-C)$ hyperconjugative mechanism, which can obscure the interpretation of the TEP values. Apart from this, the bulkiness of a phosphine ligand can overrule electronic factors; therefore, it is important to assess the steric requirements of the liagand by the cone angle θ.[1,2]

Tolman's original work was triggered by investigations by Strohmeier and co-workers[4,5] in the 1960s who investigated the σ-donor ability and π-acceptor strength of various ligand classes. Using arene chromium(0) tricarbonyl complexes in a photochemical ligand exchange reaction, they found that when the electron density on the arene ligand is increased, the electron density on the metal also increases, thus favoring back-bonding toward the CO and other ligands, which was quantified via the CO stretching frequency.

Since then, TEPs were derived from measured infrared spectra of carbonyl complexes of vanadium,[5] chromium,[6–9] molybdenum,[5,10–13] tungsten,[5,6,13–16] magnesium,[4] iron,[17–21] rhodium,[22–26] and iridium.[25,26] Computational electronic parameters (CEP) were determined using mostly density functional theory (DFT) methods.[27–32] Several review articles summarized the experimental and theoretical work in this field.[33–35]

One of the first compilations of CEPs, which included a set of 68 $LNi(CO)_3$ complexes, was published by Crabtree and co-workers.[27] These authors could show that the calculated CO stretching frequencies correlate well with the measured TEP

478

values. Gusev presented extensive compilations of CEPs for $LNi(CO)_3$, $LIrCl(CO)_2$, $LIrCp(CO)$,[28] and 76 N-heterocyclic carbene complexes.[29] In this work, he critically discussed the question whether a single parameter can adequately describe the donor properties of ligands with very diverse bonding effects. Tonner and Frenking[30] determined CEPs for a series of $LNi(CO)_3$ and $LRuCl(CO)_2$ complexes with carbene and divalent carbon(0) ligands. They could show that carbon(0) ligands CX_2, with $X = PR_3$ (carbodiphosphoranes) or NHC (carbodicarbenes) are much stronger donors than carbene and phosphine ligands. CEP values based on semiempirical calculations were published for $LMo(CO)_5$, $LW(CO)_5$, $CpRh$-$(CO)(L)$ complexes,[36] and for rhodium Vaska complexes.[37] Recently, CEPs were calculated for CO adsorption on transition metal clusters (Ni−Au).[38]

Already in the 1960s, attempts were made to relate ligand effects in metal carbonyl complexes to empirically derived force constants by applying a mathematical procedure developed by Cotton and Kraihanzel.[10,39] Cotton derived a relationship between CO bond orders and CO force constants to describe their bond strengths in $LM(CO)_5$ complexes.[10] Although empirical in nature, his approach was able to reflect the relative π-acceptor strength of various ligands, e.g., identifying PF_3 as a stronger π-accepting ligand than CO and identifying ligands such as alkylformamids as π-donors. Aubke and co-workers discussed the bond strength in the isoelectronic and isosteric series $[Au(CN)_2]^-$, $Hg(CN)_2$, and $[Au(CO)_2]^+$ based on the CN and CO stretching frequencies and force constants.[40] Other approaches to elucidate ligand effects on the CO vibrational frequencies were based on empirical ligand-specific parameters.[31,41]

Suresh and Koga suggested that the molecular electrostatic potential (MESP) provides a basis to calculate the CO stretching frequency of transition metal carbonyl complexes[42] where the usefulness of this approach has been questioned.[43] Boxer and co-workers[44] discussed the vibrational Stark effect measured by the Stark tuning rate $\Delta\mu$ on carbonyl and nitrosyl stretching frequencies in model compounds and proteins. Alyea and co-workers[45] suggested ways of differentiating between σ and π effects influencing the CO stretching frequency by referring to thermochemical data such as pK_a values. Giering combined electronic and steric effects by introducing the QALE concept (Quantitative Analysis of Ligand Effects). The original approach[46] was extended and modified over the years to provide detailed knowledge about the electronic and steric influences of phosphine ligands on metal centers.

In view of the large number of both experimental and computational investigations triggered by Tolman's concept, it seems to be generally accepted that the CO stretching frequency is a reliable parameter that reflects the electronic and steric effects of the ligands in a transition metal complex. Measured as well as calculated CO stretching frequencies refer to normal vibrational modes and these are the result of mode−mode coupling, for example, between M—C and C≡O stretching modes. There were attempts to suppress this mode coupling;[27] however, these were done incompletely. A suppression of mode−mode coupling requires two steps: (i) elimination of electronic coupling, which is done by diagonalization of the Hessian matrix and (ii) elimination of mass-coupling, for which one has to solve the mass-decoupled Euler−Lagrange equations.[47] Crabtree and co-workers[27] did only part the first step (by diagonalizing the sub-Hessian containing the $Ni(CO)_3$ unit). They failed to eliminate mass (kinematic) coupling, the importance of which is documented in this work.

In this work, we will solve this problem in a rigorous way by basing Tolman's original concept on local rather than normal vibrational frequencies. A local mode, as originally derived by Konkoli and Cremer,[47] is the true counterpart of the delocalized normal vibrational mode as was proved by Zou and co-workers.[48,49] For each bond of a molecule, the corresponding local stretching mode can be derived from calculated or experimental frequencies[50] and the associated local stretching force constant is perfectly suited to act as bond strength descriptor.[51−53] We will show that the local Tolman electronic parameter (LTEP) based on the local CO stretching frequency ω^a (LTEPw) or the local CO stretching force constant k^a (LTEPk) differs from TEP or CEP values due to mode coupling as induced by mass effects.

The results of this work are presented in the following way. In section 2, the determination of the local mode properties from experimental or calculated frequencies is summarized. In section 3, three homoleptic metal carbonyls for which all vibrational frequencies were measured will be described using the local counterparts of the normal CO stretching frequencies. This study is extended to 42 nickel−phosphine−tricarbonyl complexes in section 4 where the LTEP values obtained in this work are compared with previously published TEP and CEP values. Finally, in section 5, the conclusions of this work are summarized.

2. COMPUTATIONAL METHODS

Part of this work is based on measured vibrational frequencies and part on calculated frequencies. For the purpose of using the former to derive local mode frequencies, we shortly sketch the procedure of getting vibrational force constants based on experimental frequencies, then we derive local mode frequencies and force constants, and finally, we will utilize the latter to derive suitable parameters in the form of CO bond orders. For our derivation, we need the Wilson equation of vibrational spectroscopy:[54]

$$\mathbf{F}^q\mathbf{D} = \mathbf{G}^{-1}\mathbf{D}\Lambda \tag{1}$$

where $\mathbf{F}^q$ is the calculated force constant matrix expressed in internal coordinates q_n, $\mathbf{D}$ collects the vibrational eigenvectors $\mathbf{d}_\mu$ in form of column vectors ($\mu = 1,\cdots, N_{vib}$ with $N_{vib} = 3N - L$; N, number of atoms; L, number of translations and rotations), $\mathbf{G}$ is the Wilson G-matrix,[54] and Λ is a diagonal matrix containing the vibrational eigenvalues $\lambda_\mu = 4\pi^2 c^2 \omega_\mu^2$ where ω_μ represents the vibrational frequency of mode $\mathbf{d}_\mu$. The kinetic energy matrix $\mathbf{G}$ is determined using the atomic masses and the $\mathbf{B}$ matrix

$$\mathbf{G} = \mathbf{B}\mathbf{M}^{-1}\mathbf{B}^\dagger \tag{2}$$

where $\mathbf{B}$ is a rectangular ($N_{vib} \times 3N$) matrix containing the first derivatives of coordinates q_n with regard to the Cartesian coordinates.

For the purpose of determining the force constant matrix $\mathbf{F}^q$ from the experimental frequencies, we solve the following relationship:[50]

$$(\mathbf{F}'^q + \Delta\mathbf{F}^q)\mathbf{D}' = \mathbf{G}^{-1}\mathbf{D}'(\Lambda' + \Delta\Lambda) \tag{3}$$

where $\mathbf{F}'^q$, $\mathbf{D}'$, and Λ' are obtained from appropriate quantum chemical auxiliary calculations. The diagonal matrix $\Delta\Lambda$ is defined by the differences $\omega_\mu^{cal} - \omega_\mu^{exp}$. Hence, the unknown perturbation matrix $\Delta\mathbf{F}^q$ can be calculated from eq 4:

$$\Delta\mathbf{F}^q\mathbf{D}' = \mathbf{G}^{-1}\mathbf{D}'\Delta\Lambda \tag{4}$$

By defining $\tilde{\mathbf{D}} = \mathbf{G}^{-1/2}\mathbf{D}'$, which leads to $\tilde{\mathbf{D}}^\dagger\tilde{\mathbf{D}} = \tilde{\mathbf{D}}\tilde{\mathbf{D}}^\dagger = \mathbf{I}$ and setting $\Delta\tilde{\mathbf{F}} = \mathbf{G}^{1/2}\Delta\mathbf{F}\mathbf{G}^{1/2}$, an eigenvalue problem can be defined according to

$$\Delta\tilde{\mathbf{F}}\tilde{\mathbf{D}} = \tilde{\mathbf{D}}\Delta\Lambda \tag{5}$$
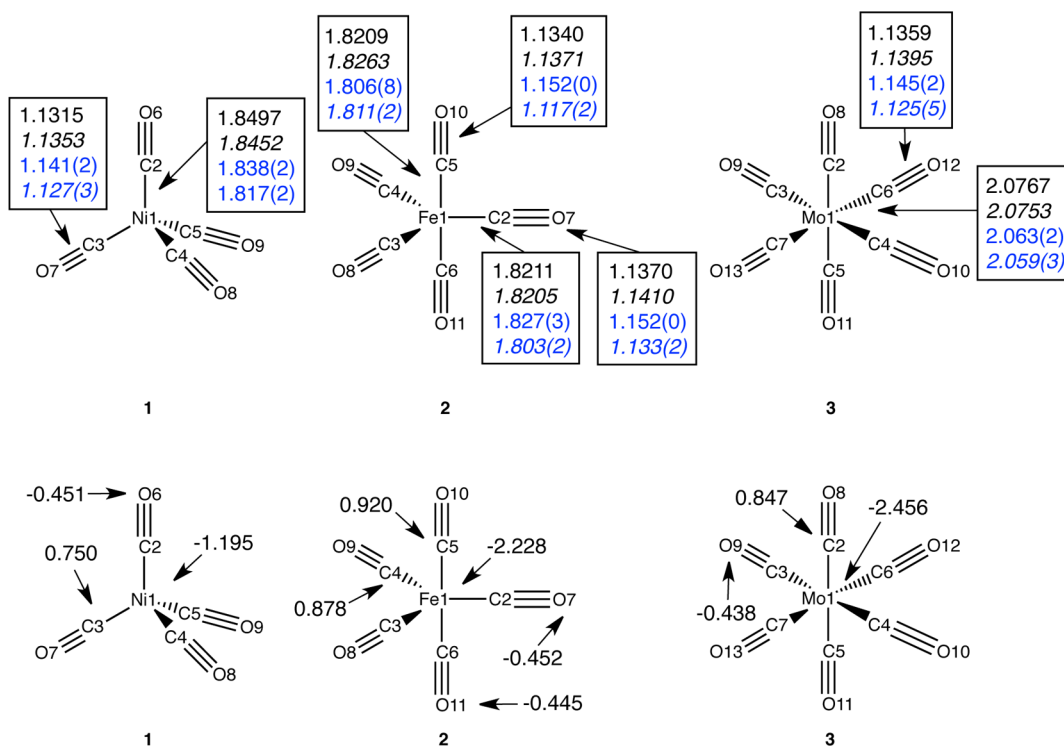
Figure 1. Geometries (upper part) and NBO charges (lower part) of metal−carbonyl compounds **1**, **2**, and **3**. Experimental bond lengths in blue; electron diffraction results in normal print; **1** from ref 73., **2** from ref 76., **3** from ref 80.; X-ray data in italics from refs 74 and 81; DFT bond lengths in black and normal print, M06; or italics, B3LYP. NBO charges obtained with M06.

which is solved by diagonalization. In this way, $\Delta\tilde{\mathbf{F}}$ and $\Delta\mathbf{F}$ are calculated and lead directly to the force constant matrix $\mathbf{F}^q$, corresponding to the experimental frequencies.

Once all matrices are available to set up eq 1, the equation is solved by standard procedures, which implies a diagonalization of matrix $\mathbf{F}^q$ to obtain the diagonal matrix $\mathbf{K}$ that provides the force constants for normal modes $\mathbf{d}_\mu$. The local vibrational mode vectors $\mathbf{a}_n$ associated with a leading parameter q_n[47] are calculated with the help of eq 6:[47−49]

$$\mathbf{a}_n = \frac{\mathbf{K}^{-1}\mathbf{d}_n^\dagger}{\mathbf{d}_n\mathbf{K}^{-1}\mathbf{d}_n^\dagger} \tag{6}$$

here $\mathbf{d}_n$ is a row vector of matrix $\mathbf{D}$. The local mode force constant k_n^a is given by eq 7:

$$k_n^a = \mathbf{a}_n^\dagger\mathbf{K}'\mathbf{a}_n \tag{7}$$

and the local mode frequency ω_n^a can be obtained from

$$(\omega_n^a)^2 = \frac{G_{nn}k_n^a}{4\pi^2c^2} \tag{8}$$

where the G-matrix element G_{nn} corresponds to the local mode mass.[47]

The above procedure is based on the assumption that the normal mode vectors of eq 1, i.e., matrix $\mathbf{D}$ can be approximated with the calculated matrix $\mathbf{D}'$ obtained within the harmonic approximation of the Wilson equation. Test calculations carried out in this work show this assumption to be reasonable. When varying method and/or basis set, the final local mode frequencies change by 10 cm^{-1} or less. Noteworthy is that the same assumption has been used successfully when scaling harmonic frequencies to obtain better approximations to measured frequencies.[55,56]

Zou and co-workers have shown that the local mode frequencies can be related to normal mode frequencies in an adiabatic connection scheme (ACS).[48] For this purpose, eq 1 is partitioned into a diagonal and an off-diagonal part. The diagonal part leads to the local mode frequencies whereas the sum of diagonal and off-diagonal part leads to the normal mode frequencies. By slowly switching on the off-diagonal part with the help of a perturbation parameter λ ($0 \leq \lambda \leq 1$), mode−mode coupling develops stepwise. If the changes in the frequencies are plotted as a function of λ, the corresponding ACS diagram reveals how mass-effects, avoided crossings (AC), etc. add to mode−mode coupling and how the local mode frequencies change.[48,49,57,58] The difference $\omega_\mu - \omega_n^a = \omega_{\text{coup}}$ leads to the coupling frequencies ω_{coup}. They can be tested by the zero-point energy (ZPE) condition

$$\text{ZPE(normal)} = \text{ZPE(local)} + \text{ZPE(coup)} \tag{9}$$

where ZPE(local) and ZPE(coup) correspond to the ZPE values calculated with local mode and coupling frequencies, respectively.[48,49]

For an N-atom molecule of a given point-group symmetry, the N_{vib} normal vibrational modes are exactly defined, which, however, is not the case for local vibrational modes. Because a given local mode is independent of all other local modes (which leads to the advantage that it is not dependent on the way the molecular geometry is described), one can start with any redundant set of internal coordinates to set up the ACS. However, when increasing $\lambda = 0 \rightarrow 1$ only those local mode frequencies, the mode vectors of which have the largest overlap with the normal vibrational modes, converge to frequencies ω_μ whereas all other local mode frequencies converge to zero. In this way, a unique set of N_{vib} local vibrational modes is selected.

In previous work, the local stretching force constants were used as relative bond strength descriptors, which can be applied in form of a bond order n.[52,53,59] This implies the definition of suitable reference bonds with defined n-values. In this work, we use the CO bond in methanol and that in formaldehyde as reference bonds with $n = 1$ and $n = 2$, respectively. Utilizing the extended Badger rule,[52,60] we have shown that the bond order is related to the local stretching force constant k^a by a power relationship of the type $n = a(k^a)^b$ where constants a and b are obtained using the two reference bonds and the condition that for a force constant of zero the bond order also is zero. A bond order relationship based on the experimental frequencies of methanol and formaldehyde[61] was derived to determine the CO bond orders of the homoleptic carbonyl complexes Ni(CO)$_4$ (**1**), Fe(CO)$_5$

Table 1. Experimental Normal Mode Frequencies ω_μ and the Corresponding Local Mode Force Constants k_n^a and Frequencies ω_n^a of Ni(CO)$_4$ (1)^a

μ	symmetry	ω_μ [cm^{-1}]	#	parameter	k^a [mdyn Å^{-1}]	ω^a [cm^{-1}]	ω_{comp} [cm^{-1}]
21	A_1	2132	8	C5−O9	17.195	2063.2	69.2
20	T_2	2058	7	C4−O8	17.195	2063.2	−5.4
19	T_2	2058	6	C3−O7	17.195	2063.2	−5.4
18	T_2	2058	5	C2−O6	17.195	2063.2	−5.4
17	T_2	459	4	Ni1−C5	1.900	569.5	−110.6
16	T_2	459	3	Ni1−C4	1.900	569.5	−110.6
15	T_2	459	2	Ni1−C3	1.900	569.5	−110.6
14	T_2	423	21	Ni1−C5−O9	0.152	293.1	130.0
13	T_2	423	20	Ni1−C4−O8	0.152	293.1	130.0
12	T_2	423	19	Ni1−C3−O7	0.152	293.1	130.0
11	E	380	18	Ni1−C2−O6	0.152	293.1	86.9
10	E	380	17	Ni1−C5−O9	0.152	293.1	86.9
9	A_1	371	1	Ni1−C2	1.900	569.5	−198.7
8	T_1	300	16	Ni1−C4−O8	0.152	293.1	6.9
7	T_1	300	15	Ni1−C3−O7	0.152	293.1	6.9
6	T_1	300	14	Ni1−C2−O6	0.152	293.1	6.9
5	T_2	80	13	C3−Ni1−C5	0.360	195.3	−115.3
4	T_2	80	12	C3−Ni1−C4	0.360	195.3	−115.3
3	T_2	80	11	C2−Ni1−C5	0.360	195.3	−115.3
2	E	62	10	C2−Ni1−C4	0.360	195.3	−133.3
1	E	62	9	C2−Ni1−C3	0.360	195.3	−133.3
ZPE [kcal/mol]:		19.08				19.80	−0.72

^{a}For each local mode, the driving internal coordinate and the coupling frequencies ω_{coup} is given. Zero-point energies (ZPE) are added to verify the ZPE-additivity requirement ZPE(total) = ZPE(local) + ZPE(coup). Bending and torsional force constants are given in mdyn Å/rad^2. For a numbering of atoms, see Figure 1.

(2), and Mo(CO)$_6$ (3) (see Figure 1) where the parameters of the bond order relationship were determined as $a = 0.351$; $b = 0.694$.

DFT calculations were carried out with the B3LYP functional[62,63] and the M06 functional of Truhlar and co-workers[64] employing the aug-cc-pVTZ basis set of Dunning and co-workers.[65,66] Using M06, the bond order relationship derived is given by $a = 0.327$ and $b = 0.686$. The normal vibrational modes of all molecules investigated in this work were analyzed in terms of local vibrational modes using the CNM (characterizing normal modes) approach by Konkoli and Cremer[67] as integrated in the quantum chemical program package COLOGNE2013.[68] In this work, the results of the CNM analysis are presented in the form of bar diagrams, which give the contributions of the various local modes to a specific normal mode (in %) in form of color-coded ranges for a given bar.

3. ANALYSIS OF THE VIBRATIONAL FREQUENCIES OF NI(CO)$_4$, FE(CO)$_5$, AND MO(CO)$_6$

In Tables 1−3, the experimental frequencies for 1,[69,70] 2,[71] and 3[72] are listed. For each normal mode, frequency ω_μ, the corresponding local mode force constants k_n^a and frequency ω_n^a, the parameter, which drives the local mode (given according to the notation in Figure 1), and the coupling frequency ω_{coup}, which provides a measure of mode−mode coupling, are given. The zero point energy condition is fulfilled in all three cases: ZPE(normal) = ZPE(local) + ZPE(coup). In Figures 2 and 3, the vibrational normal modes of 1 are analyzed with the help of a normal mode decomposition diagram and the ACS between local and normal frequencies. For 2, the same analysis is provided in Figures 4 and 5 whereas Figures 6 and 7 summarize results for 3.

Nickel Tetracarbonyl (1). In Figure 1, experimental geometries of 1[73,74] are compared with M06 (black, normal print) and B3LYP geometries (black italics), which are bracketed by the gas phase result (NiC, 1.838; CO, 1.141

Å)[73] and the solid state result (NiC, 1.817; CO, 1.127 Å).[74] NBO charges are given in the lower half of Figure 1.

The four highest frequencies of 1 (Table 1, Figure 3) correspond to the four CO stretching frequencies split up into a single A_1-symmetrical normal stretching mode (#21) at 2132 cm^{-1} and three T_2-symmetrical modes at 2058 cm^{-1} (splitting: 75 cm^{-1}). All four frequencies emerge from one local mode frequency at 2063 cm^{-1} (see Figure 3), which is significantly (112 cm^{-1}) lower than that of free CO (2170 cm^{-1}) whereas the frequency of normal mode 21 is only 38 cm^{-1} smaller than that of free CO. The lowering of the local CO stretching frequency is the result of σ-donation and π-back-donation involving the Ni and the CO molecular orbitals (MOs) where the back-donation from Ni to CO requires the t_2 and e-symmetrical 3d(Ni) orbitals.

Clearly, by using the normal CO stretching frequency of the A_1-symmetrical mode as a bond strength descriptor, the full amount of CO weakening cannot be correctly described because of a mass-dependent splitting of A_1- and T_2-symmetrical modes. Another deficiency of the normal mode frequencies becomes apparent when the mode decomposition of the CO stretching modes in terms of local modes are analyzed (see Figure 2). All CO stretching modes couple with the NiC stretching modes, leading to a non-negligable admixture of about 4%. This leads to coupling contributions to the CO stretching frequencies and obscures the description of the CO bond strength.

The local NiC stretching frequencies are at 570 cm^{-1} whereas the normal mode frequencies are at 459 (T_2) and 371 cm^{-1} (A_1). There is an avoided crossing between the NiC stretching and NiCO bending modes at $\lambda = 0.97$, which leads to mode−mode mixing and makes it difficult to assess from the vibrational spectrum information on the NiC bond. However,

Table 2. Experimental Normal Mode Frequencies ω_μ and the Corresponding Local Mode Force Constants k_n^a and Frequencies ω_n^a of Fe(CO)$_5$ (2)^a

μ	symmetry	ω_μ [cm^{-1}]	#	parameter	k^a [mdyn Å^{-1}]	ω^a [cm^{-1}]	ω_{comp} [cm^{-1}]
27	A_1'	2121	10	C6–O11	16.924	2046.8	74.2
26	A_1'	2042	8	C4–O9	16.456	2018.3	23.7
25	A_2''	2034	9	C5–O10	16.924	2046.8	−12.8
24	E'	2013	7	C3–O8	16.456	2018.3	−5.3
23	E'	2013	6	C2–O7	16.456	2018.3	−5.3
22	E'	645	3	Fe1–C4	2.458	649.8	−4.8
21	E'	645	2	Fe1–C3	2.458	649.8	−4.8
20	A_2''	619	5	Fe1–C6	2.510	656.6	−37.6
19	E''	543	27	Fe1–C6–O11	0.427	402.3	140.7
18	E''	543	26	Fe1–C5–O10	0.427	402.3	140.7
17	E'	488	22	Fe1–C6–O11	0.427	402.3	85.7
16	E'	488	21	Fe1–C5–O10	0.427	402.3	85.7
15	A_2''	474	25	Fe1–C4–O9	0.258	360.5	113.5
14	A_1'	443	4	Fe1–C5	2.510	656.6	−213.6
13	E'	429	23	Fe1–C2–O7	0.379	378.7	50.3
12	E'	429	20	Fe1–C4–O9	0.379	378.7	50.3
11	A_1'	413	1	Fe1–C2	2.458	649.8	−236.8
10	A_2'	383	19	Fe1–C3–O8	0.379	378.7	4.3
9	E''	375	24	Fe1–C3–O8	0.258	360.5	14.5
8	E''	375	18	Fe1–C2–O7	0.344	360.5	14.5
7	A_2''	105	15	C4–Fe1–C5	0.703	269.5	−164.5
6	E'	100	17	C5–Fe1–C6	0.439	230.5	−130.5
5	E'	100	16	C5–Fe1–C6	0.438	230.5	−130.5
4	E''	97	14	C3–Fe1–C5	0.703	269.5	−172.5
3	E''	97	13	C2–Fe1–C5	0.703	269.5	−172.5
2	E'	64	12	C2–Fe1–C4	0.301	184.4	−120.4
1	E'	64	11	C2–Fe1–C3	0.301	184.4	−120.4
	ZPE [kcal/mol]:	25.94				26.98	−1.05

^{a}For each local mode, the driving internal coordinate and the coupling frequencies ω_{coup} is given. Zero-point energies (ZPE) are added to verify the ZPE-additivity requirement ZPE(total) = ZPE(local) + ZPE(coup). Bending and torsional force constants are given in mdyn Å/rad^2. For a numbering of atoms, see Figure 1.

the local NiC stretching force constant of 1.900 mdyn/Å reveals that the metal−C bond is relatively weak, which is in line with a measured BDE (bond dissociation energy) of just 25 ± 2 kcal/mol for **1**.[75]

Iron Pentacarbonyl (2). Some DFT methods (M06, BPW91) describe the axial (ax) FeC bond as being slightly shorter than the equatorial (eq) FeC bond (M06: 1.8209 (ax) vs 1.8211 Å (eq); see Figure 1), which is confirmed by the electron diffraction result in the gas phase (1.806 (ax) vs 1.827 Å (eq)[76] but not by the X-ray diffraction analysis.[74] In line with the X-ray results (1.811 (ax) vs 1.803 Å (eq)), other DFT XC functionals (B3LYP, BP86) predict the equatorial bonds to be slightly shorter (B3LYP: 1.8263 (ax) vs 1.8205 Å (eq)). Similarly, confusing results have been found by other authors.[77,78]

The local CO stretching frequencies of the ax- and eq-positioned ligands are 2047 and 2018 cm^{-1}, respectively, thus indicating that the eq-CO bonds are somewhat weaker than the ax ones in line with DFT bond lengths of 1.137 (eq) vs 1.134 (ax, M06) and 1.141 (eq) vs 1.137 Å (ax, B3LYP) and local CO stretching force constants of 16.456 (eq) and 16.924 mdyn/Å (ax, Table 2). Normally, a weaker CO bond indicates stronger π-back-donation from the metal atom, which should be reflected by a stronger FeC bond and stretching force constant. The values for the ax-FeC bonds are $\omega^a = 657$ cm^{-1} and $k^a = 2.510$ mdyn/Å. For the eq-FeC bonds, they are 650 cm^{-1} and

2.458 mdyn/Å (see Table 2), respectively, i.e., a slightly stronger axial FeC is connected to a slightly stronger CO bond.

Irrespective of the description of ax and eq bond lengths, experimental frequencies and all DFT XC frequencies calculated in this work always lead to a larger force constant for the ax-FeC bonds, provided the local vibrational modes are derived from the normal vibrational modes (see Supporting Information). This confirms that the vibrational properties are much more sensitive to changes in bond strength than measured or calculated bond lengths, provided one has the local mode data available. The latter reflect the curvature of the PES (potential energy surface) at the equilibrium minimum; therefore, they are directly related to the bond strength whereas the bond length is only indirectly related to the bond strength and is, accordingly, not reliable.

The local mode properties show that (i) π-back-donation should be stronger for **2** than for **1** and (ii) the relative strength of the FeC bonds is no longer in line with the common explanation that π-back-donation from the metal atom leads to strengthening of the metal−carbon and a weakening of the CO bond: NiC, $k^a = 1.900$; ax-FeC, 2.510; eq-FeC, 2.458 mdyn/Å and (Ni)CO, 17.195; ax-(Fe)CO, 16.924; eq-(Fe)CO, 16.456 mdyn/AA (see Tables 1 and 2). Observation i can be explained, considering the larger electronegativity of Ni ($\chi = 1.75$) compared to that of Fe (1.64[79]), which is in line with the fact that the HOMO of **1** is lower in energy than that of **2**. Hence, the higher lying Fe(3d)-HOMO and the fact that Fe is more

Table 3. Experimental Normal Mode Frequencies ω_μ and the Corresponding Local Mode Force Constants k_n^a and Frequencies ω_n^a of Mo(CO)$_6$ (3)^a

μ	sym.	ω_μ [cm^{-1}]	#	param.	k^a [mdyn Å^{-1}]	ω^a [cm^{-1}]	ω_{coup} [cm^{-1}]
33	A_{1g}	2121	7	C2−O8	16.482	2020	101
32	E_g	2025	11	C6−O12	16.482	2020	5
31	E_g	2025	8	C3−O9	16.482	2020	5
30	T_{1u}	2003	10	C5−O11	16.482	2020	−17
29	T_{1u}	2003	9	C4−O10	16.482	2020	−17
28	T_{1u}	2003	12	C7−O13	16.482	2020	−17
27	T_{1u}	596	19	Mo1−C2−O8 (y)	0.326	336	260
26	T_{1u}	596	23	Mo1−C6−O12 (y)	0.326	336	260
25	T_{1u}	596	17	Mo1−C6−O12 (x)	0.326	336	260
24	T_{2u}	507	16	Mo1−C5−O11 (x)	0.326	336	171
23	T_{2u}	507	15	Mo1−C4−O10 (x)	0.326	336	171
22	T_{2u}	507	20	Mo1−C3−O9 (y)	0.326	336	171
21	T_{2g}	477	14	Mo1−C3−O9 (x)	0.326	336	141
20	T_{2g}	477	21	Mo1−C4−O10 (y)	0.326	336	141
19	T_{2g}	477	22	Mo1−C5−O11 (y)	0.326	336	141
18	A_{1g}	391	1	Mo1−C2	1.782	532	−141
17	E_g	381	5	Mo1−C6	1.782	532	−151
16	E_g	381	2	Mo1−C3	1.782	532	−151
15	T_{1u}	367	4	Mo1−C5	1.782	532	−165
14	T_{1u}	367	6	Mo1−C7	1.782	532	−165
13	T_{1u}	367	3	Mo1−C4	1.782	532	−165
12	T_{1g}	342	18	Mo1−C7−O13 (x)	0.326	336	6
11	T_{1g}	342	24	Mo1−C7−O13 (y)	0.326	336	6
10	T_{1g}	342	13	Mo1−C2−O8 (x)	0.326	336	6
9	T_{1u}	82	32	C3−Mo1−C5	0.541	200	−118
8	T_{1u}	82	30	C4−Mo1−C7	0.541	200	−118
7	T_{1u}	82	25	C2−Mo1−C6	0.541	200	−118
6	T_{2g}	79	28	C3−Mo1−C6	0.541	200	−121
5	T_{2g}	79	26	C6−Mo1−C5	0.541	200	−121
4	T_{2g}	79	31	C2−Mo1−C3	0.541	200	−121
3	T_{2u}	60	29	C6−Mo1−C4	0.541	200	−140
2	T_{2u}	60	27	C5−Mo1−C7	0.541	200	−140
1	T_{2u}	60	33	C5−Mo1−C4	0.541	200	−140
ZPE [kcal/mol]:		29.82				30.23	−0.40

^{a}For each local mode, the driving internal coordinate and the coupling frequencies ω_{coup} is given. Zero-point energies (ZPE) are added to verify the ZPE-additivity requirement ZPE(total) = ZPE(local) + ZPE(coup). Bending and torsional force constants are given in mdyn Å/rad^2. For a numbering of atoms, see Figure 1.

negatively charged (−2.288 vs −1.195 e; Figure 1) explain that Fe donates electron density to an empty $\pi^\star$(CO) MO better than Ni, thus weakening the CO bonds more, as reflected by the local CO streching force constants and frequencies.

The σ-donation from the CO ligand to the metal involves, for the ax ligands, the 3d$_{z^2}$(Fe) orbital and, for the eq CO ligands, the 3d$_{xy}$(Fe) orbitals. Overlap is better for the former than the latter (L−Ni−L angle, 120°; lobe angle, 90°). Accordingly, the axial CO ligands should be stronger σ-donors (confirmed by the charges shown in Figure 1) and establish stronger FeC bonds, which obviously is more effective than bond strengthening via π-back-donation.

In the ACS of **2**, mode coupling causes a splitting of the ax-CO frequencies by 87 cm^{-1} and that of the eq-CO frequencies by 29 cm^{-1}, which leads to a crossing of the $A_1{}'$ (axial) and $A_2{}''$ (eq) frequencies (see Figure 5). The larger splitting of the ax-CO stretches is a consequence of the coaxial alignment of their mode vectors compared to an unfavorable angle of 120° (a 90° arrangement would suppress any coupling) enclosed by the eq-CO mode vectors. In both cases, mode coupling involves the

FeC stretching modes which, because of this, contribute to the CO normal modes (Figure 4).

The normal mode FeC stretchings range from 443 (axial) to 645 cm^{-1} (eq) and are difficult to characterize without the local vibrational modes because they mix among each other, with the various bending modes and also with the CO stretching modes. It is important to note that the splitting of the CO stretching frequencies depends on the symmetry of the molecule, the closeness of the local mode vectors in the molecule, the direction of the mode vectors (strong coupling if an angle of 0 or 180° is enclosed, no coupling if the angle is 90°), and the ratio of the masses involved. These factors change from molecule to molecule; therefore, the splitting of the CO stretching frequencies is different (74 in **1**; 87 and 29 cm^{-1} in **2**) as well as the coupling frequencies for the symmetrical CO stretching modes (69, 74, and 24 cm^{-1}). This makes the use of the frequencies of the A_1-symmetrical modes for diagnostic purposes questionable.

Molybdenum Hexacarbonyl (3). We have included in our analysis a complex with an element of the second transition metal period, which has a different number of CO ligands and,
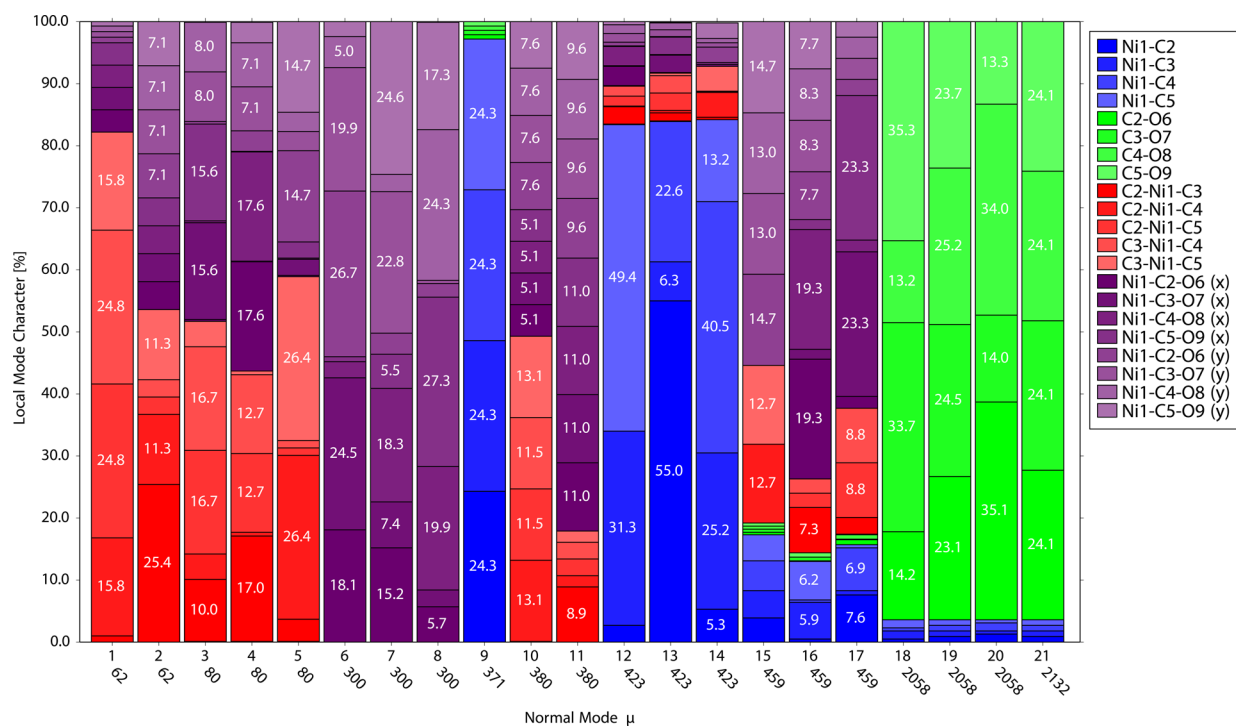
Figure 2. Characterization of the normal modes of Ni(CO)$_4$ in terms of local mode contributions. Each of the 21 normal mode vectors, $\mathbf{d}_\mu$, is represented by a bar (mode number and experimental frequencies are given at the bottom of each bar), which is decomposed in terms of 21 local mode vectors, $\mathbf{a}_n$. The local mode parameters are presented in form of a color code (right side of diagram; for numbering of atoms, see Figure 1). Contributions larger than 5% are given within the partial bars representing a local mode.

accordingly, a different symmetry. The experiment[80,81] and theory are in line with regard to the geometry of **3** (see Figure 1).

The local CO stretching frequencies and force constants of **3** are 2020 cm^{-1} and 16.482 mdyn/Å. This indicates that the CO bonds are comparable to those in **2**. π-Back donation is as strong as in **2**, which is in line with an electronegativity χ(Mo) = 1.30[79] and an NBO charge of Mo in **3** of -2.456 e (Figure 1). The local force constants reveal that the MoC bonds are weak (1.782 mdyn/Å), which reflects the fact that the magnitude of the $4d\pi$(Mo)$-2p\pi$(C) overlap is reduced (MoC bond length: 2.063 Å[80]).

The normal CO stretching frequencies are at 2121 (A_{1g}), 2025 (E_g), and 2003 cm^{-1} (T_{1u}) where the coupling frequencies are 101, 5, and -17 cm^{-1} leading to a splitting of 118 cm^{-1} (Figure 7). Although the highly symmetrical CO stretching frequency can be easily identified as in the case of **1** and **2**, it alone cannot reflect the properties of the CO bond in **3** as these are disguised by mode–mode couplings. Clearly if these change due to an exchange of one of the CO ligands by another ligand, the mode coupling situation becomes more complicated.

The local MoC stretching frequencies are at 532 cm^{-1}, corresponding to a force constant of 1.782 mdyn/Å. Due to mode couplings with bending modes and avoided crossings with the latter (Figure 7), the corresponding normal mode frequencies spread in the range 367–391 cm^{-1}, which are easy to analyze once the local mode frequencies are obtained.

Although the number of data points is too small to be statistically relevant, it is interesting to note that local and normal mode CO stretching frequencies correlate only with significant scattering ($R^2 = 0.85$) where the same is true for a correlation between local CO frequencies and calculated CO bond lengths (see Supporting Information). Both normal mode

frequencies and bond lengths are at best qualitative descriptors of the changes in the bond strength of CO; therefore, they are also not suitable as reliable electronic parameters as Tolman had originally hoped. However, we will show in the following that Tolman's original idea is very useful, provided one converts normal mode frequencies into local mode frequencies.

4. EXTENSION OF TOLMAN'S CONCEPT: THE LOCAL TOLMAN ELECTRONIC PARAMETER (LTEP)

In this section, we will introduce the local TEP (LTEP) based on the local properties of the vibrational modes. As obvious from the discussion above, such an LTEP can be easily applied to different carbonyl complexes as it is no longer constrained to a given class of carbonyls such as the nickel–phosphine carbonyls.[1,2] Special efforts were made by Crabtree and co-workers[27] to establish a computational counterpart to the TEP coined CEP, which both confirmed and extended the usefulness of the TEP. Therefore, we will focus in this work on a subset of the nickel-tricarbonyl complexes LNi(CO)$_3$ used by Crabtree and co-workers[27] (see Figure 8) to demonstrate the usefulness of the TEPs.

In Figure 9, measured and M06-calculated vibrational frequencies for **1**, **2**, and **3** are compared. They agree reasonably with a standard deviation of 9.9 cm^{-1} and an R^2 of 0.9997. However, more important is the comparison of measured and calculated CO stretching frequencies, which leads to a standard deviation of just 3.0 cm^{-1}. This result implies that it is straightforward to scale calculated CO stretching frequencies by a suitable scaling factor derived from Ni(CO)$_4$ to obtain CEP and LTEP values close to TEP and the corresponding experimentally based LTEP values, respectively.

In Table 4, the vibrational properties of the nickel–tricarbonyl complexes **L1**−**L42** are listed and compared with
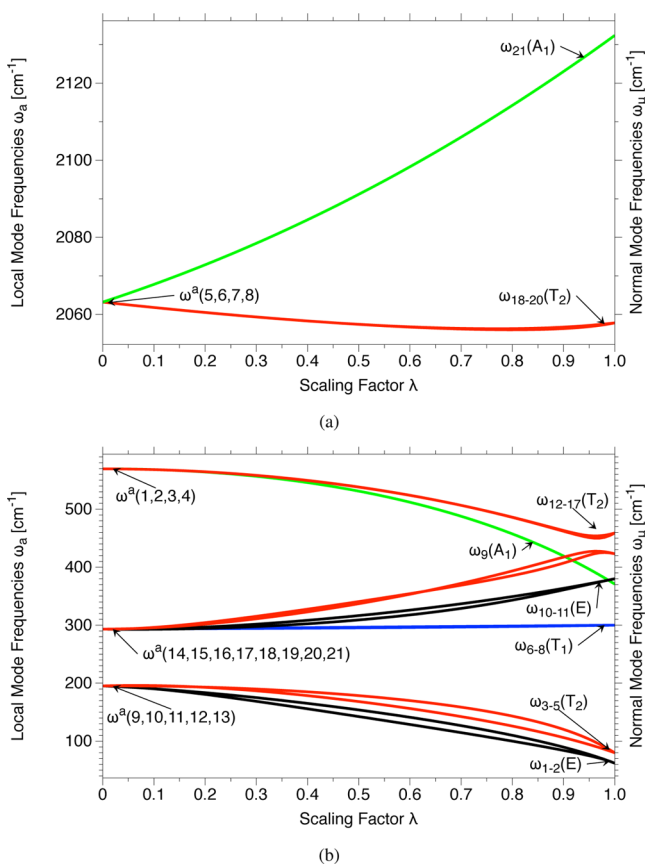
Figure 3. Adiabatic connection scheme of $Ni(CO)_4$ (**1**) based on experimental frequencies. Panels a and b show the upper and lower frequency ranges, respectively. For symmetries and the notation of normal mode as well as local mode frequencies, see Table 1. Compare also with Figure 1.

the measured TEP literature values taken from Crabtree and co-workers.[27] For each ligand L, the calculated CO bond length r, the calculated CEP and its scaled counterpart, $\overline{CEP}$, the local CO stretching frequency ω^a, its scaled value $\overline{\omega}^a$, the corresponding force constant k^a, and the bond order n based on the latter are given. The scale factor was determined from measured and calculated frequencies of $Ni(CO)_4$ (see Table 4) and applied to correct (at least approximately) for anharmonicity effects. For the same reason, $\overline{\omega}^a$ values were determined. Especially important is the coupling frequency ω_{coup} because the latter reveals the deviation of the CEP (or TEP) from its electronic value due to mode coupling. Also given are electron density and energy density at the CO bond critical point as they may also reflect the strength of the CO bond and by this the degree of π-back-donation.

Comparison of TEP, CEP, and LTEP. For the 42 ligands chosen, the TEP varies by 208 cm^{-1} in the range 1981 to 2189 cm^{-1}, i.e., by 10%. Similar values are obtained for CEP and $\overline{CEP}$ (see Table 4). Positively charged L lead to high TEP values because they withdraw electronic charge from Ni and reduce π-back-donation to the CO ligands yielding high CO stretching frequencies. Anionic ligands donate electronic charge to the Ni atom and increase its π-back-donation, yielding low TEP values. In view of the accuracy of the measured frequencies and their sensitivity to the ligand L, the usefulness of the TEP and CEP is convincing.

However, the coupling frequencies ω_{coup} for **L1−L42** vary by 78 cm^{-1} from 22 to 100 cm^{-1} revealing that, even for the CO stretching modes of the highest symmetry, mode−mode coupling cannot be neglected and, accordingly, CEP and TEP provide qualitative rather than quantitative measures of the electronic effect of ligand L. The LTEP defined by the local CO stretching mode ω^a is always smaller than TEP (or CEP) and varies by 284 (scaled: 271) cm^{-1} or 13% from 2282 (2184) to 1998 (1913) cm^{-1}. It is more sensitive than the TEP or CEP as their mode−mode coupling leads to a dampening of electronic effects.

In Figure 10, the TEP and $\overline{CEP}$ are compared with the LTEP. As already indicated by the coupling frequencies, the scattering of both TEP and $\overline{CEP}$ values is relatively large ($R^2 =$ 0.985 and 0.970, respectively). The calculated standard deviations are 5.4 and 8.0 cm^{-1}. Strong deviations are found for both anionic and neutral ligands L. The ascend of the correlation line is smaller than 1, which corresponds to the fact that the sensitivity of TEP and $\overline{CEP}$ is not as large as that of the LTEP. Both **1** and free CO deviate distinctly from the correlation shown in Figure 10.

The vibrational frequency is an observable, i.e., it can be directly measured. However, its use as an electronic parameter is problematic because it depends on the masses of the atoms involved in a vibration. Since Tolman focused on just the CO group, the mass effect on the frequency may be considered as being constant, thus establishing the TEP as a true electronic parameter. This argument falls short if the ligand L lowers the symmetry from C_{3v} to C_s or even C_1, which leads to new coupling situations with different reduced masses. Hence, the use of TEP or CEP for a ligand L leading to any symmetry is flawed by mass effects. This, of course, no longer holds for the local CO stretching frequencies, which always depend on the same reduced mass defined by a single CO ligand.

Nevertheless, it is desirable to assign to the frequency-based LTEP the corresponding local force constant k^a, which is also given in Table 4. The local CO stretching force constants change by 26.% (4.91 mdyn/Å) from 16.127 to 21.037 mdyn/Å) and thus, they are much more sensitive than the CO stretching frequencies. As in previous work, we have converted the local stretching force constant, which is an excellent bond strength descriptor, into a bond order n for easier use (see Figure 11).[49,52,53,59] The CO bond orders $n(CO)$ for ligands **L1−L42** change from 2.638 to 2.198 and by varying 18% in dependence of ligand L from a strong, closer to a triple bond to a weak, closer to a double bond (see Table 4 and Figure 11). The value of free CO is 2.563 and for **1** = **L3**, 2.439 (see Table 4).

The bond order, based on the local stretching force constant, has to be used in connection with the local CO stretching frequency to establish a general LTEP, which can easily be extended to ligands other than CO as probes for the electronic structure of a transition metal complex. For simplicity reasons, we distinguish between the two parameters by LTEPw and LTEPn, respectively.

In previous studies in the literature, little emphasis has been laid on the length of the CO bond as it was considered to be too insensitive. The calculated r values of Table 4 reveal that the CO length changes from 1.1165 to 1.1515 Å, i.e., just 3% or 0.0350 Å, which is too small to be reliably reproduced by experimental means instead of the computational tools used in this work. When the calculated CO bond lengths are correlated
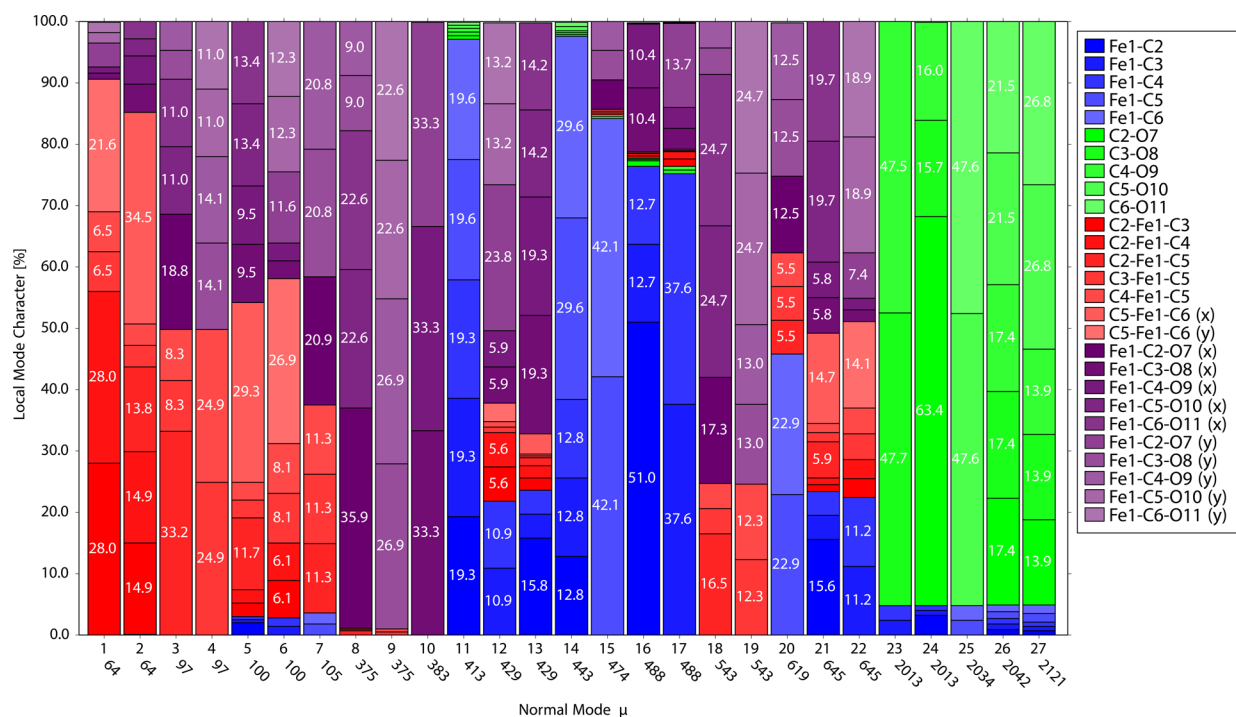
Figure 4. Characterization of the normal modes of $Fe(CO)_5$ in terms of local mode contributions. Each of the 27 normal mode vectors, $\mathbf{d}_\mu$ is represented by a bar (mode number and experimental frequencies are given at the bottom of each bar), which is decomposed in terms of 27 local mode vectors, $\mathbf{a}_n$. The local mode parameters are presented in form of a color code (right side of diagram; for numbering of atoms, see Figure 1. Contributions larger than 5% are given within the partial bars representing a local mode.

with the CO bond orders n (Supporting Information), the scattering of the r values is substantial and does not suggest to use r as a quantitative CO bond strength descriptor.

Cremer and Kraka[82,83] demonstrated that the bond strength is also reflected by the electron and energy density at a bond critical point $\mathbf{r}_c$ ($\rho_c = \rho(\mathbf{r}_c)$ and $H_c = H(\mathbf{r}_c)$) where a negative electron density indicates a covalent bond. Indeed, there is a linear relationship between n and these two quantities (see Supporting Information); however, again the scattering is too large to consider these relationships more than semiquantative.

Most important is that the LTEP changes the order of electronic effects obtained with the TEP or CEP, which is indicated in Table 4 by reordering ligands according to their LTEP (the numbering of complexes is done using the TEP values of Crabtree and co-workers.[27] This will be discussed in the next subsection.

In Figure 12, MO interaction diagrams are shown, which are used to rationalize the various ligand effects. They are made by choosing a suitable coordinate system, e.g., the z-direction as the direction of the Ni−L bond, the xy-plane perpendicular to the Ni-L direction, and the x-direction in the direction of one of the CO ligands when this is projected into the xy-plane. In this way, one of the CO ligands is in the xz-plane and one can distinguish between an in-plane (ip) and two out-of-plane (oop) CO ligands. Furthermore, we will distinguish for C_{3v}-symmetrical ligands, such as AX_3, between ecclipsed or staggered CO ligands.

Using this coordinate system, σ-donation of the ligand is into the $3d_{z^2}(Ni)$ or the $4p_z(Ni)$ orbital. The Ni-atom has a $3d^8 4s^2$ electron configuration whereas, in Ni complexes, one considers a $3d^{10} 4s^0$ configuration and expects the four ligands to fill up the 4s4p orbitals to obtain the 18-electron configuration of Ar in the valence shell. Hence, one can consider σ- or π-donation

to either polarize the distribution of the 3d electrons or increase the amount of negative charge at the Ni atom by filling "empty" 3d(Ni) orbitals. The latter choice facilitates the discussion as it is simpler to explain back-donation via the 3d orbitals than by constructing linear combinations of 4p(Ni) orbitals that suit the same purpose.

For the coordinate system chosen, π-back-donation to CO can proceed via the $3d_{z^2}(Ni)$ orbital by a direct overlap with the $\pi^\star$ orbital of the ip CO or an indirect mechanism caused by an increase of the electron density at Ni via the $3d_{x^2+y^2}(Ni)$ orbital (see panels b and e in Figure 12). It is obvious that by choosing a different coordinate system, orbitals $3d_{z^2}$ and $3d_{x^2+y^2}$ would exchange their role; however, the overall π-back-donation result would be the same. On the basis of the coordinate system given in Figure 12, we will rationalize the electronic effects of the different ligands L utilizing the LTEP values of Table 4. Our analysis will be guided by the LTEP values rather than the PMO (perturbational MO) analysis; however, we will use the latter to test for any contradictions between LTEP and PMO description.

Cationic Ligands. The electron withdrawing ability of a cationic ligand will diminish the chance of π-back-donation into the empty $\pi^\star$(CO) orbitals; therefore, strong CO bonds, as reflected by high LTEP values, result. One would expect that the electron withdrawing ability of ligand $O{=}N^+$ (**L1**) is larger than that of $H−C^+$ (**L2**). However, ligand **L2** has one electron less and thereby an empty pπ orbital (assuming that both ligands establish a σ-donor bond to Ni) for accepting negative charge from Ni (π-back-donation to L). We calculate a NiC(H) local stretching force constant k^a of 5.077 mdyn/Å compared to a Ni−N value of 3.876 mdyn/Å in **L1**. Hence, **L2** more effectively withdraws negative charge from Ni and accordingly reduces π-back-donation to CO to a minimum, which leads to
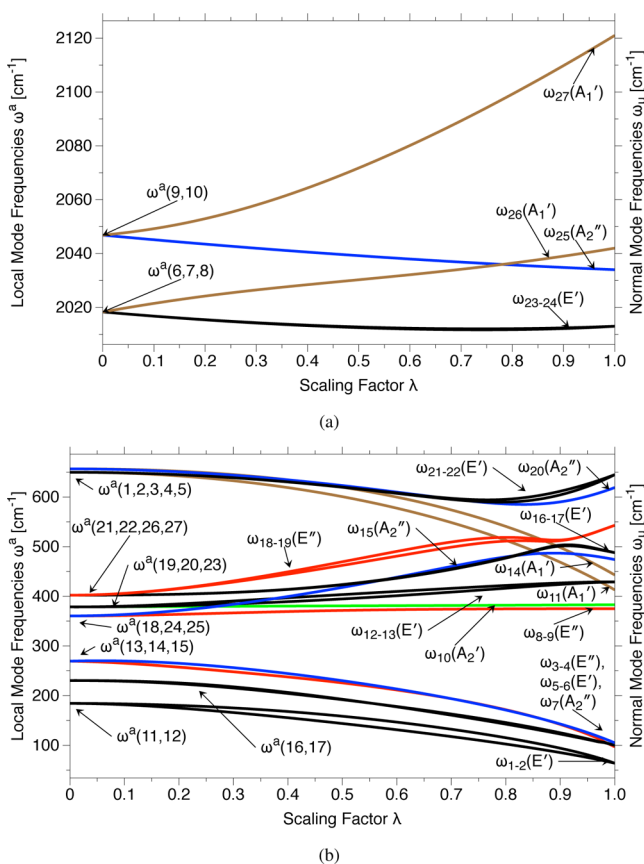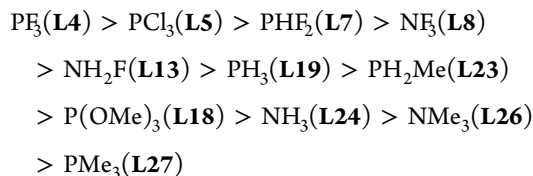
(a)

(b)

Figure 5. Adiabatic connection scheme of Fe(CO)$_5$ (**2**) based on experimental frequencies. Panels a and b show the upper and lower frequency ranges, respectively. For symmetries and the notation of normal mode as well as local mode frequencies, see Table 2. Compare also with Figure 1.

the largest LTEP values found for the 42 complexes investigated in this work. The TEP and CEP values based on normal CO stretching frequencies lead to an incorrect order of the two ligands.

Neutral Ligands. Comparing phosphine with amine ligands leads to a unexpected order of electron withdrawing abilities:

$$PF_3(\mathbf{L4}) > PCl_3(\mathbf{L5}) > PHF_2(\mathbf{L7}) > NF_3(\mathbf{L8})$$

$$> NH_2F(\mathbf{L13}) > PH_3(\mathbf{L19}) > PH_2Me(\mathbf{L23})$$

$$> P(OMe)_3(\mathbf{L18}) > NH_3(\mathbf{L24}) > NMe_3(\mathbf{L26})$$

$$> PMe_3(\mathbf{L27})$$

where averaged LTEP values are taken if the symmetry, due to the ligand L, is reduced to C_s. Obviously, phosphines are stronger electron withdrawing from Ni than amines. This has to do with the σ-donor and π-acceptor ability of AX$_3$ (A = P or N; X = H, halogen, Me). Clearly, PF$_3$ is a better σ-donor (involving the electron lone pair) than NF$_3$ due to the lower electronegativity of P compared to N. Both molecules are π-acceptors involving the $\sigma^\star$(AX) orbitals (see panel d in Figure 12). For PF$_3$, the latter are in the range of the 3d(Ni) orbitals whereas, for NF$_3$, these are lower in energy because two rather than just one electronegative atom is involved. The difference in σ-donation and dπ-acceptance leads to a much stronger PNi bond (k^a = 1.338 mdyn/Å) in **L4** than the NNi bond (k^a = 0.078 mdyn/Å) in **L8**.
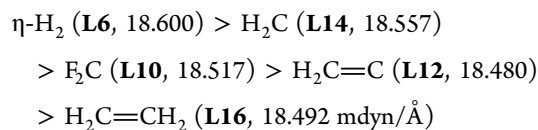
The importance of the $\sigma^\star$(AX) acceptor ability (one could also speak of pseudo-$\pi^\star$ orbitals as normally done in the case of AX$_3$ groups) becomes obvious when considering the PCl$_3$ ligand. This is definitely a better σ-donor than PF$_3$; however, it is also a weaker dπ-acceptor because the $\sigma^\star$(PCl) orbitals are higher in energy for the less electronegative Cl atoms. The NiP bond of **L5** is weaker (k^a = 0.997 mdyn/Å) than that of **L4**. PCl$_3$ is less electron withdrawing, which gives Ni a somewhat higher chance of back-donating into the CO orbitals. The same conclusions can be drawn using the polarization picture discussed above.

The electron withdrawing ability of L becomes smaller with decreasing numbers of halogen atoms bonded to P or N. Methyl groups raise the $\sigma^\star$ orbitals. If the methyl groups are bonded to an electronegative atom such as N, the dπ electron withdrawing ability is somewhat larger than when the methyl groups are linked to the more electropositive P atom. It is interesting to note that also individual LTEP values can be observed for the three CO groups when the symmetry is lowered to C_s as in **L7**, **L13**, or **L23**. For example, in **L7** the LTEPw and LTEPn values are higher for those CO groups that are eclipsed with the PF bonds, which confirms the preferred π-back-donation into the $\sigma^\star$(PF) orbital and therefore, less into the eclipsed CO bonds, thus leading to their higher CO bond strength as reflected by the LTEP values.

The ordering of all AX$_3$ ligands shown above and based on the associated LTEP values can be easily rationalized in terms of the orbital interaction rules. Only in the case of **L18**, does the TEP-CEP ordering deviate from the LTEP ordering. The P(OMe)$_3$ ligand (as in the case of PF$_3$) has lower lying $\sigma^\star$(PO) orbitals for accepting 3d density from Ni; therefore, its LTEP values are higher than those of PMe$_3$. However, the methyl groups reduce this effect so that **L18** takes an intermediate position between **L19** and **L27**, which is not correctly described by the TEP and CEP values.

Carbenes :CX$_2$ can establish strong bonds with Ni as in the case of ligand **L14** (k^a = 2.600 mdyn/Å), which possesses (for a positioning of the X substituents in the yz-plane) an empty p$_x\pi$ orbital. Hence, the NiCX$_2$ bond results from σ-sp^2(C) donation to the 3d$_{z^2}$ orbital and pπ-acceptance from an occupied 3d$_{xz}$ orbital. This has a different effect on the three CO groups: the ip CO group (perpendicular to :CX$_2$) can more strongly donate to the partially emptied 3d$_{xz}$(Ni) orbital, with which it overlaps strongly (contrary to the two oop CO groups, see panel c in Figure 12). The NiC bond becomes much stronger (k^a = 1.961 mdyn/Å compared to k^a = 1.335 mdyn/Å in the case of **L7**). π-Back donation via the 3d$_{x^2+y^2}$(Ni) orbital affects only the oop CO groups, which obtain lower LTEP values.

We find the following LTEP order for carbenes and some related ligands where averaged values are used when the CO ligands are different because of the C_s symmetry:

$$\eta\text{-H}_2\ (\mathbf{L6},\ 18.600) > \text{H}_2\text{C}\ (\mathbf{L14},\ 18.557)$$

$$> \text{F}_2\text{C}\ (\mathbf{L10},\ 18.517) > \text{H}_2\text{C}{=}\text{C}\ (\mathbf{L12},\ 18.480)$$

$$> \text{H}_2\text{C}{=}\text{CH}_2\ (\mathbf{L16},\ 18.492\ \text{mdyn/Å})$$

For difluorocarbene, the empty $2p_x\pi$ orbital is lowered in energy due to the F substituents, which should lead to a stronger withdrawal of 3d$_{xz}$(Ni) density than in the case of methylene. However, the $2p_x\pi$ orbital is partially filled with π-density from the F atoms and, accordingly, the electron withdrawal ability of CF$_2$ is lower than that of CH$_2$ as is the σ-
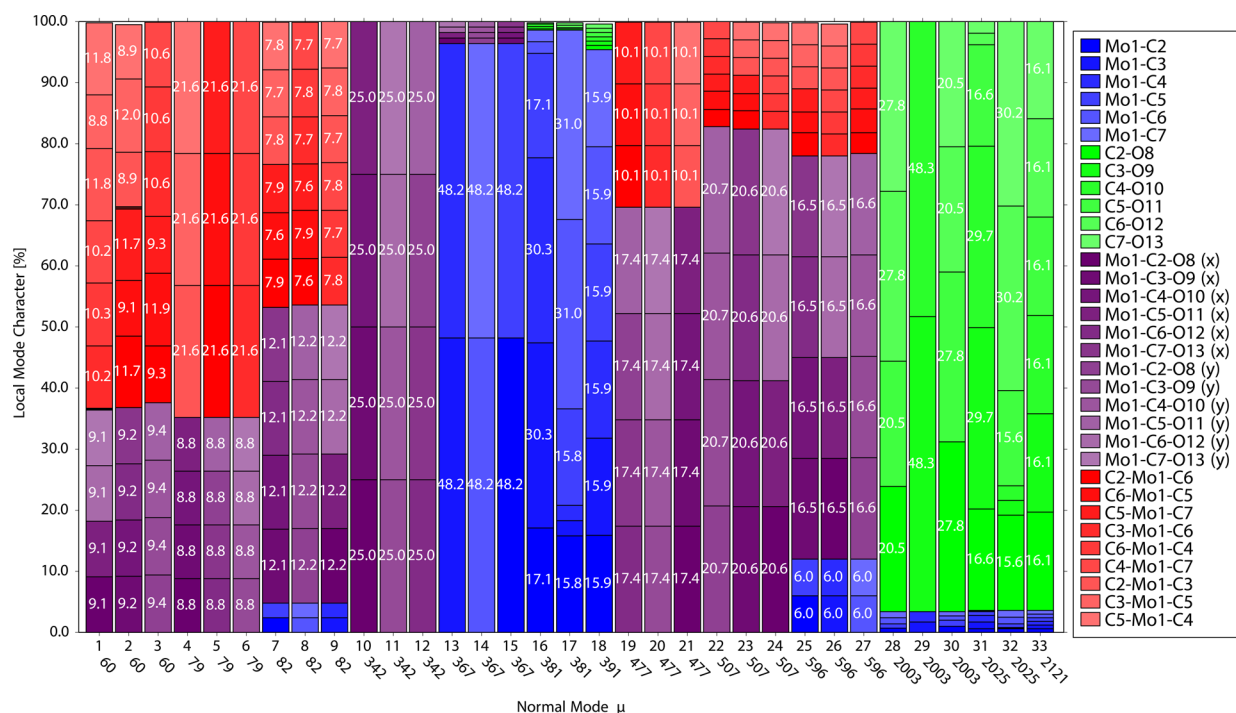
Figure 6. Characterization of the normal modes of $Mo(CO)_6$ in terms of local mode contributions. Each of the 33 normal mode vectors, $\mathbf{d}_\mu$, is represented by a bar (mode number and experimental frequencies are given at the bottom of each bar), which is decomposed in terms of 33 local mode vectors, $\mathbf{a}_n$. The local mode parameters are presented in form of a color code (right side of diagram; for numbering of atoms, see Figure 1. Contributions larger than 5% are given within the partial bars representing a local mode.

donor ability because of the electronegative F substituents (k^a = 1.863 mdyn/Å compared to 2.600 mdyn/Å in the case of CH_2). Methylene establishes a stronger NiC bond, increases the strength of the σ-NiC bond of the ip CO (because of stronger $3d_{xz}$(Ni) density withdrawal), and leads to stronger π-back-donation via the $3d_{z^2}$(Ni) orbital (see panel b in Figure 12).

The oop NiC bonds do not benefit from the withdrawal of $3d_{xz}$(Ni) density; therefore, they are weaker. π-Back-donation in the oop CO bonds proceeds via the $3d_{x^2+y^2}$ orbital (see panel e in Figure 12), which is affected by exchange repulsion with the σ(CF) electrons. Therefore, π-back-donation into the $\pi^\star$ orbitals of the oop CO ligands is stronger for **L10** than for **L14** and lower LTEP values result in the former case. Similar explanations hold for the LTEP values when a vinylidene ligand is used where, however, an empty $2p_y\pi$(C) orbital has to be considered.

The η-HH ligand is a weak σ-donor but, via its $\sigma^\star$ orbital, is a good $3d\pi$-acceptor (see f) in Figure 12), which leads to a lengthening of the HH bond to 0.805 Å. This leads to a strong NiC bond for the eclipsed CO ligand (k^a = 2.056 mdyn/Å compared to 1.552 for the oop NiC bonds) and a consequential CO bond strengthening reflected by higher LTEP values. Because the σ-donor and $\sigma^\star$-acceptor ability of η-HH balance each other largely, Ni remains to be a weak π-back-donor for the oop CO ligands involving the $3d_{x^2+y^2}$ electrons thus yielding somewhat lower LTEP values.

The η-ethene ligand adopts a position along the y-axis (see panels g and h in Figure 12). In this position, it can effectively interact with the $3d_{x^2+y^2}$ orbital so that the latter can accept negative charge from the π(CC) orbital, thus increasing its π-back-donation ability: the oop CO ligands adopt clearly lower LTEP values than when interacting with the η-HH ligand.

The importance of the orbital energy for assessing the potential π-acceptor ability of a ligand becomes obvious in the following series:

$$O\equiv C\ (\mathbf{L3}) > S\equiv C\ (\mathbf{L9}) > N\equiv N\ (\mathbf{L11})$$
$$> HC\equiv N\ (\mathbf{L21}) > MeC\equiv N\ (\mathbf{L22})$$
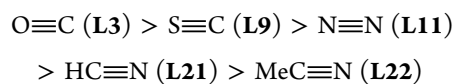
Clearly, CO has a lower $\pi^\star$ energy than N_2, which makes it a better acceptor, whereas its σ-donor ability is larger than that of N_2. Therefore, L in **L11** withdraws less density from Ni and π-back-donation leads to lower LTEP values for the $Ni(CO)_3$ unit. In the case of the CS group, the $\pi^\star$ orbital has an energy between that of CO and N_2, which leads to intermediate LTEP values.

The change from an NN to a HCN ligand implies an increased σ-donor ability whereas the π-acceptor abilities remain comparably small. An increase in σ-donation into the $3d_{z^2}$(Ni) orbital also increases the π-back-donation ability of Ni (see panel b in Figure 12) and leads to lower LTEP values. This trend is continued if a methyl group donates electron density via hyperconjugation to the nitrile group as in **L22**.

The σ–π-donor trends can be side-tracked by geometrical features. The ligand H_2S should be a stronger σ- and π-donor than H_2O. However, it adopts a tilted form where neither its σ nor its π lone pair orbital is pointing toward the Ni atom. This orientation makes an anomeric delocalization of the electron lone pairs into the $\sigma^\star$(NiC) orbitals possible, thus strengthening the NiS bond (k^a = 0.399 mdyn/Å), which is significantly stronger than the Ni–O bond (k^a = 0.151 mdyn/Å) in **L15** where the H_2O ligand is not tilted, donates density from both σ(O) and π(O) lone pair orbital and consequently causes the LTEP values to be lower than in **L20**. For dimethylether, this effect is enhanced because of electron density donation from the methyl groups caused by hyperconjugation.
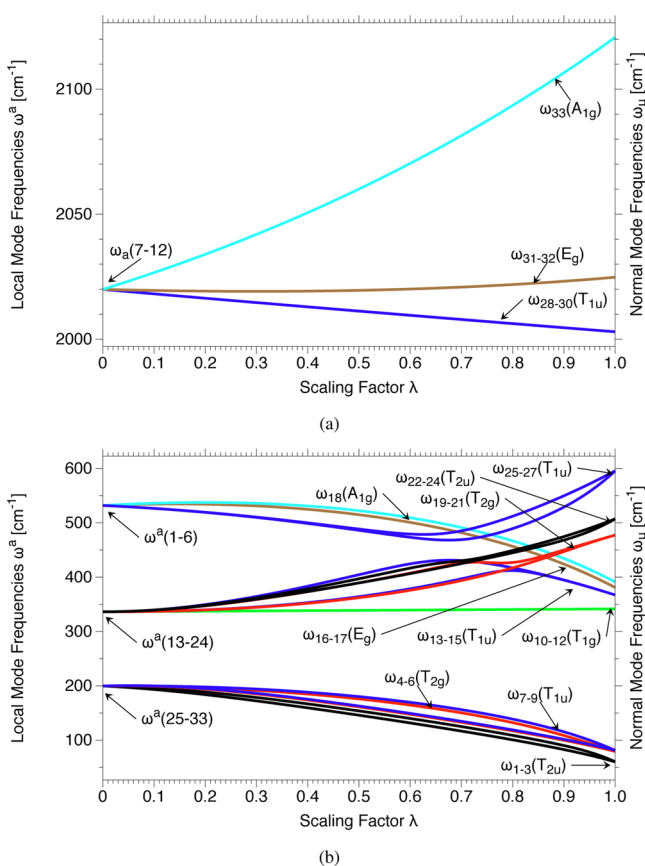
(a)

(b)

Figure 7. Adiabatic connection scheme (ACS) of $Mo(CO)_6$ (**3**) based on experimental frequencies. Panels a and b show the upper and lower frequency ranges, respectively. For symmetries and the notation of normal mode as well as local mode frequencies, see Table 3. Compare also with Figure 1.

For dimethylthioether, electrostatic effects cause an opposite tilting. Hyperconjugation leads to a lowering of the a'-symmetrical $3p\pi(S)$ lone pair orbital, which therefore, can mix with the a'-symmetrical $\sigma(S)$ lone pair orbital to become a strong donor orbital donating negative charge to the $3d_{z^2}(Ni)$ orbital. This leads to stronger π-back-donation to the $\pi^\star(CO)$ orbital and lower LEP values. The following order, contrary to that obtained by the TEP (CEP) values, results:

$$H_2S \ (\mathbf{L20}) > H_2O \ (\mathbf{L15}) > Me_2O \ (\mathbf{L17}) > Me_2S \ (\mathbf{L25})$$
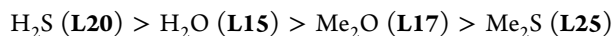
Anionic Ligands. Especially for anions, it becomes obvious (see Table 4) that both TEP and CEP do not provide the same order of ligand effects given by the LTEP values. For example, the LTEP parameters clearly indicate that Ni π-back-donation to CO increases for halogen ligands X^- if the atomic number of X decreases:

$$I^- \ (\mathbf{L30}) > Br^- \ (\mathbf{L31}) > Cl^- \ (\mathbf{L29}) > F^- \ (\mathbf{L34})$$
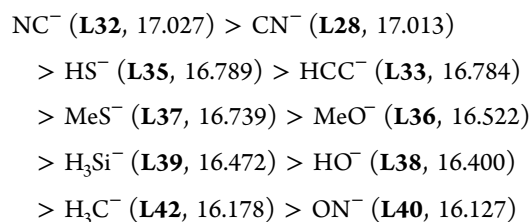$$> H^- \ (\mathbf{L41})$$
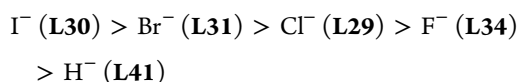
where H^- has been included in this series. At first glance, this may be unexpected because the electron withdrawing ability of F is clearly larger than that of I. However, in the anions, the XNi stretching force constant increases from 0.557 (I), 0.650 (Br), 0.732 (Cl), 1.218 (F) to 1.401 (H), thus indicating that the XNi bond strength increases with decreasing atomic number. Hydrogen has a much lower electron affinity (0.75

eV^{84}) than F (3.40 eV) or the other halogens. Accordingly, the hydride anion is a strong donor and the charge is accepted via the $3d_{z^2}(Ni)$ orbital, which implies back-donation into the antibonding CO $\pi^\star$ orbitals as discussed above (see panel b in Figure 12). Accordingly, relatively strong NiC (k^a = 2.466 mdyn/Å) and weak CO bonds (k^a = 16.224 mdyn/Å) are obtained.

In the case of F^-, σ-donation is weaker in view of its larger electron affinity. Also, there is $p\pi(F)$-donation to the $3d_{xz}(Ni)$ and $3d_{yz}(Ni)$ orbitals, which causes weakening of the NiC bonds (σ-CO donation is reduced) whereas the CO bonds are somewhat stronger (compared to **L41**) due to reduced π-back-donation. As the atomic number of halogen X increased, overlap between the np(X) and 3d(Ni) orbitals is decreased and the HOMO energy of X^- raises above that of the 3d(Ni) orbitals so that σ and $p\pi$-donation both become weaker, which causes a stepwise increase of the NiC and CO bond strength. The LTEP values can reflect only one of these electronic effects however by complementing them by the NiL and NiC stretching force constants the existence of the two effects is verified.

For the other anionic ligands, the following order is given by the LTEP values (based on averaged values in the case of C_s rather than C_{3v} symmetry):

$$NC^- \ (\mathbf{L32}, \ 17.027) > CN^- \ (\mathbf{L28}, \ 17.013)$$
$$> HS^- \ (\mathbf{L35}, \ 16.789) > HCC^- \ (\mathbf{L33}, \ 16.784)$$
$$> MeS^- \ (\mathbf{L37}, \ 16.739) > MeO^- \ (\mathbf{L36}, \ 16.522)$$
$$> H_3Si^- \ (\mathbf{L39}, \ 16.472) > HO^- \ (\mathbf{L38}, \ 16.400)$$
$$> H_3C^- \ (\mathbf{L42}, \ 16.178) > ON^- \ (\mathbf{L40}, \ 16.127)$$

which differs significantly from the one given by the TEP (or CEP) values. This series confirms some effects already discussed: (i) a negatively charged second row atom is a stronger donor than a negatively charged third row atom, which has to do with the energy of the HOMO and the orbital overlap (too high and diffuse, respectively, for the latter). Therefore, **L42** leads to lower LTEP values than **L39** and **L38** to a lower than **L35**. (ii) A methyl group increases the donor ability of the ligand due to hyperconjugation as in **L37** or **L36**. (iii) A triple bond is a weaker donor (because of sp hybridization and increased electronegativity) than a double bond (sp^2 hybridization). This explains the lower LTEP values of **L40** compared to **L28**. Secondary effects arise from the electronegativity of the triple bond partner. The LTEP values are lower for **L33** than for **L32** because, in the latter case, the electronegativity of the N atom makes the nitrile atom a weaker donor.

In summary, the LTEP values are in line with the electronic effects to be expected on the basis of PMO theory and accordingly are more reliable than any electronic parameter based on the normal CO stretching frequency, which via mode−mode coupling includes electronic effects of neighboring atoms and/or groups.

5. CHEMICAL RELEVANCE: DIRECT ANALYSIS AND JUSTIFICATION OF THE TOLMAN ELECTRONIC PARAMETER

The TEP provides indirect information about the strength of the ligand-transition metal interaction whereas the local mode approach presented in this work provides the direct information about the Ni−L bond strength in form of the
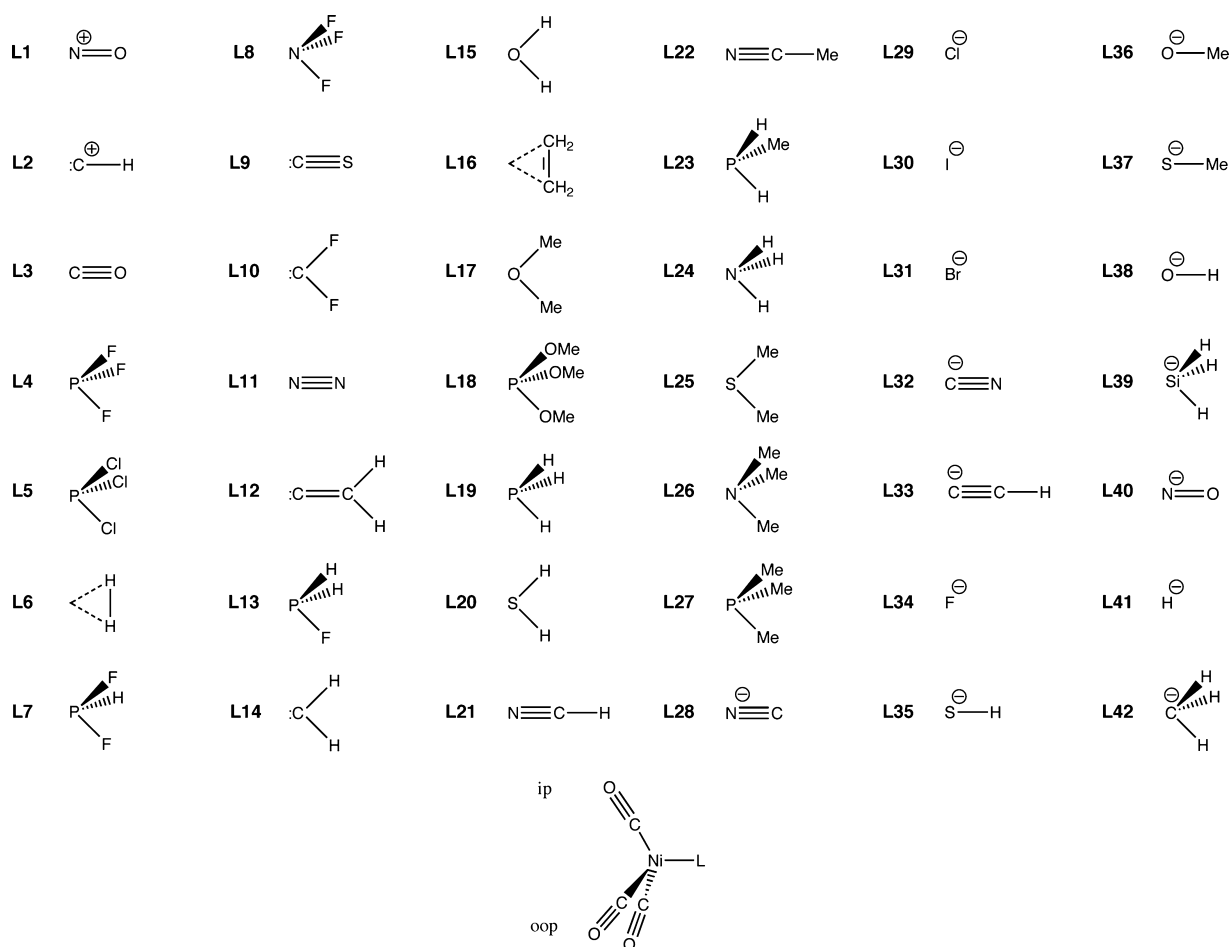
Figure 8. Nickel−carbonyl complexes LNiCO$_3$ **L1−L42** studied in this work.
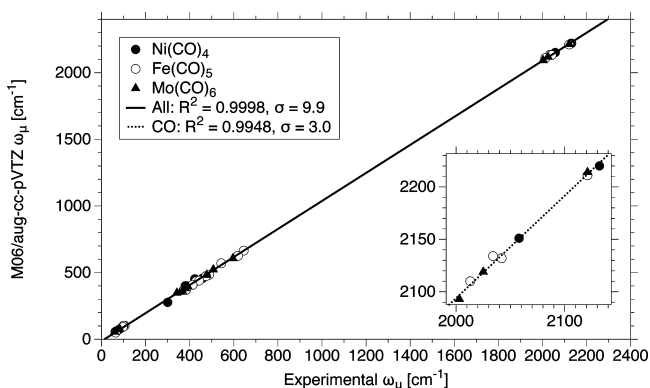

Figure 9. Correlation of calculated with measured normal mode frequencies ω_μ including all frequencies or just the CO stretching frequencies (inset). M06/aug-cc-pVTZ calculations.

local Ni−L bond stretching force constants k^a(NiL). Hence, all information is available to directly test the reliably of the TEP.

The TEP is based on the assumptions that the A_1-symmetrical CO stretching frequency of LNi(CO)$_3$ is only slightly affected by mode coupling effects and that it reflects the donor/acceptor activity of L, i.e., σ or π bonding effects of L change the density at Ni, which is reflected via π-back-donation by the CO stretching frequency. The coupling frequencies listed in Tables 1−4 (experimentally or computationally based) range from 20 to 100 cm^{-1} and indicate that the first assumption is at best of qualitative nature.

With regard to the second assumption, three additional considerations have to be made. (i) Frequencies are mass-dependent and therefore not reliable if the electronic effects of different ligands and transition metals are compared. Local modes derived either from measured or calculated frequencies lead to local force constants, which are better electronic parameters because they do not depend on masses. (ii) The TEP depends critically on the assumption that the M−L bonding interactions lead to change in the NiC bonding interactions, which is correctly reflected by the CO stretching frequency irrespective of whether σ or π bonding effects are involved. iii) Tolman[2] invented a cone angle as a measure for the bulkiness of a ligand. Bulky ligands establish weaker bonding to the transition metal, which can be anticipated from the value of the cone angle. The local mode stretching force constant reflects all changes in bonding whether caused by steric or other environmental effects; therefore, an extra steric parameter is not needed. Interactions between bulky ligands can quantitatively be accessed by the local bending force constants.

Hence, it remains to test the quantitative validity of the TEP by clarifying whether a change in the M−L bonding interactions is correctly reflected by the CO bond strength. This is possible with local mode force constants, which are quantitative and reliable measures of bond strength.[51−53] Just as the CO local stretching force constants are available, so too are the NiL local mode stretching force constants.

Table 4. Electronic Parameters LTEP, CEP, and TEP for Complexes L1−L42 Based on CO Stretching Properties[a]

complex	ligand	symmetry	r(CO)	$k^a(CO)$ LTEPk	$\omega^a(CO)$ LTEPw	$\bar{\omega}^a(CO)$	$\omega_{coup}(CO)$	TEP[27]	CEP	$\overline{CEP}$	$n(CO)$ LTEPn	ρ_c	H_c
			[Å]	[mdyne Å^{-1}]	[cm^{-1}]	[cm^{-1}]	[cm^{-1}]	[cm^{-1}]	[cm^{-1}]	[cm^{-1}]		[e Å^{-3}]	[Hartree Å^{-3}]
L2	CH$^+$	C$_{3v}$	1.1165	21.037	2282.1	2184.4	22.4	2189.5	2304.5	2213.2	2.638	3.451	−6.429
L1	NO$^+$	C$_{3v}$	1.1170	20.964	2278.1	2180.6	27.5	2193.5	2305.6	2214.3	2.632	3.449	−6.425
L4	PF$_3$	C$_3$	1.1312	18.830	2159.0	2066.6	47.9	2110.8	2206.9	2119.5	2.445	3.333	−6.136
L3	CO	Td	1.1315	18.768	2155.5	2063.2	64.9	2120.0	2220.4	2132.5	2.439	3.330	−6.130
L5	PCl$_3$	C$_{3v}$	1.1312	18.762	2155.1	2062.9	46.8	2107.0	2201.9	2114.7	2.439	3.332	−6.135
L9	CS	C$_{3v}$	1.1315	18.729	2153.2	2061.0	44.7	2097.7	2197.9	2110.8	2.436	3.329	−6.128
L7−2	PHF$_2$	C$_s$	1.1320	18.707	2152.0	2059.9	46.6				2.434	3.326	−6.120
L10−1	CF$_2$	C$_s$	1.1326	18.619	2146.9	2055.0	51.9	2097.1	2198.8	2111.7	2.426	3.320	−6.104
L12−1	CCH$_2$	C$_s$	1.1326	18.603	2145.9	2054.1	49.6	2094.1	2195.5	2108.5	2.425	3.319	−6.102
L6−1	η^2-H$_2$	C$_s$	1.1331	18.600	2145.8	2054.0	57.5	2102.6	2203.3	2116.0	2.424	3.316	−6.094
L13−1	PH$_2$F	C$_s$	1.1328	18.598	2145.7	2053.9	45.6	2090.9	2191.3	2104.5	2.424	3.319	−6.102
L14−1	CH$_2$	C$_s$	1.1326	18.589	2145.2	2053.4	48.4	2089.3	2193.6	2106.8	2.423	3.318	−6.096
L6−2	η^2-H$_2$	C$_s$	1.1327	18.580	2144.6	2052.8	58.7				2.422	3.320	−6.105
L7−1	PHF$_2$	C$_s$	1.1330	18.579	2144.6	2052.8	54.0	2100.8	2198.6	2111.5	2.422	3.318	−6.100
L11	σ-N$_2$	C$_{3v}$	1.1330	18.576	2144.4	2052.6	52.4	2096.3	2196.8	2109.8	2.422	3.318	−6.098
L14−2	CH$_2$	C$_s$	1.1319	18.541	2142.4	2050.7	51.2				2.419	3.325	−6.119
L8	NF$_3$	C$_3$	1.1337	18.506	2140.3	2048.7	62.2	2100.2	2202.5	2115.3	2.416	3.311	−6.081
L10−2	CF$_2$	C$_s$	1.1318	18.466	2138.0	2046.5	60.8				2.412	3.327	−6.124
L12−2	CCH$_2$	C$_s$	1.1316	18.419	2135.3	2043.9	60.2				2.408	3.329	−6.128
L13−2	PH$_2$F	C$_s$	1.1338	18.409	2134.7	2043.3	56.6				2.407	3.311	−6.084
L16−1	C$_2$H$_4$	C$_s$	1.1336	18.408	2134.7	2043.3	50.4	2083.6	2185.1	2098.6	2.407	3.313	−6.090
L16−2	C$_2$H$_4$	C$_s$	1.1347	18.354	2131.6	2040.4	53.5				2.402	3.303	−6.063
L19	PH$_3$	C$_{3v}$	1.1349	18.326	2129.9	2038.7	53.3	2083.2	2183.2	2096.7	2.400	3.302	−6.060
L23−2	PH$_2$Me	C$_s$	1.1354	18.250	2125.5	2034.5	51.8				2.393	3.298	−6.050
L20−2	H$_2$S	C$_s$	1.1356	18.245	2125.2	2034.2	58.0				2.392	3.296	−6.043
L21	NCH	C$_{3v}$	1.1355	18.233	2124.5	2033.6	51.8	2078.9	2176.3	2090.1	2.391	3.297	−6.047
L15−2	H$_2$O	C$_s$	1.1352	18.204	2122.9	2032.0	68.7				2.389	3.299	−6.049
L20−1	H$_2$S	C$_s$	1.1358	18.196	2122.4	2031.6	60.8	2081.3	2183.2	2096.7	2.388	3.294	−6.039
L18	P(OMe)$_3$	C$_3$	1.1358	18.141	2119.2	2028.5	56.0	2079.5	2175.2	2089.1	2.383	3.296	−6.045
L17−1	Me$_2$O	C$_s$	1.1365	18.120	2118.0	2027.3	71.5	2082.9	2189.5	2102.8	2.381	3.289	−6.024
L15−1	H$_2$O	C$_s$	1.1366	18.115	2117.6	2027.0	74.0	2085.3	2191.6	2104.8	2.381	3.287	−6.020
L25−2	Me$_2$S	C$_s$	1.1364	18.115	2117.6	2027.0	56.2				2.381	3.290	−6.029
L22	NCMe	C$_{3v}$	1.1364	18.106	2117.1	2026.5	59.9	2078.5	2177.0	2090.8	2.380	3.289	−6.028
L23−1	PH$_2$Me	C$_s$	1.1364	18.095	2116.5	2025.9	60.8	2075.3	2177.3	2091.1	2.379	3.290	−6.031
L17−2	Me$_2$O	C$_s$	1.1355	18.039	2113.2	2022.8	76.3				2.374	3.296	−6.043
L24	NH$_3$	C$_{3v}$	1.1376	17.991	2110.4	2020.1	64.2	2073.3	2174.6	2088.5	2.370	3.280	−6.004
L26	NMe$_3$	C$_{3v}$	1.1377	17.937	2107.2	2017.0	64.4	2067.6	2171.6	2085.6	2.365	3.279	−6.001
L27−1	PMe$_3$	C$_{3v}$	1.1373	17.925	2106.5	2016.3	59.1	2064.1	2165.6	2079.8	2.364	3.283	−6.013
L27−2	PMe$_3$	C$_{3v}$	1.1373	17.910	2105.6	2015.5	60.0				2.362	3.283	−6.013
L25−1	Me$_2$S	C$_s$	1.1376	17.907	2105.4	2015.3	68.4	2072.8	2173.8	2087.8	2.362	3.281	−6.007
L30[b]	I$^-$	C$_{3v}$	1.1436	17.079	2056.2	1968.2	68.6	2033.6	2124.8	2040.7	2.287	3.124	−5.426
L32	CN$^-$	C$_{3v}$	1.1443	17.027	2053.1	1965.2	69.3	2028.5	2122.4	2038.4	2.282	3.224	−5.866
L28	NC$^-$	C$_{3v}$	1.1436	17.013	2052.2	1964.4	78.3	2035.1	2130.5	2046.1	2.280	3.229	−5.879
L31	Br$^-$	C$_{3v}$	1.1438	16.994	2051.1	1963.3	76.2	2033.5	2127.3	2043.1	2.279	3.227	−5.874
L29	Cl$^-$	C$_{3v}$	1.1440	16.915	2046.3	1958.7	81.4	2034.0	2127.7	2043.4	2.271	3.225	−5.869
L35−2	SH$^-$	C$_s$	1.1454	16.818	2040.4	1953.1	69.9				2.263	3.214	−5.841
L33	HCC$^-$	C$_{3v}$	1.1461	16.784	2038.3	1951.1	75.2	2020.5	2113.5	2029.8	2.259	3.209	−5.829
L37−2	MeS$^-$	C$_s$	1.1460	16.755	2036.6	1949.4	68.0				2.257	3.209	−5.828
L35−1	SH$^-$	C$_s$	1.1468	16.732	2035.2	1948.1	75.1	2016.5	2110.3	2026.8	2.255	3.203	−5.813
L37−1	MeS$^-$	C$_s$	1.1470	16.708	2033.7	1946.7	70.9	2011.3	2104.6	2021.3	2.252	3.201	−5.808
L38−1	OH$^-$	C$_s$	1.1465	16.612	2027.9	1941.1	77.3	2006.4	2105.2	2021.8	2.243	3.204	−5.816
L36−1	MeO$^-$	C$_s$	1.1463	16.539	2023.4	1936.8	88.6	2013.2	2112.0	2028.4	2.237	3.206	−5.822
L36−2	MeO$^-$	C$_s$	1.1461	16.513	2021.8	1935.3	90.2				2.234	3.208	−5.827
L39	SiH$_3^-$	C$_3$	1.1491	16.472	2019.3	1932.9	52.1	2005.2	2071.4	1989.3	2.230	3.184	−5.766
L34	F$^-$	C$_{3v}$	1.1460	16.465	2018.9	1932.5	99.6	2016.8	2118.5	2034.6	2.230	3.209	−5.829
L38−2	OH$^-$	C$_s$	1.1479	16.294	2008.4	1922.4	96.8				2.214	3.194	−5.791
L41	H$^-$	C$_{3v}$	1.1515	16.224	2004.1	1918.3	73.7	1989.5	2077.8	1995.5	2.207	3.165	−5.719
L40−1	NO$^-$	C$_s$	1.1498	16.191	2002.1	1916.4	77.4	1990.4	2079.5	1997.1	2.204	3.176	−5.743
L42	CH3$^-$	C$_{3v}$	1.1515	16.178	2001.2	1915.5	72.0	1981.3	2073.2	1991.1	2.203	3.164	−5.716
L40−2	NO$^-$	C$_s$	1.1498	16.127	1998.1	1912.6	81.4				2.198	3.176	−5.743
CO		C$_{\infty v}$	1.1236	20.170	2234.4	2076.9	0.0				2.563	3.396	−6.284

Table 4. continued

[a]The L numbering follows the TEP values; however, the ligands are ordered according to the LTEP values obtained in this work so that the differences between the two electronic parameters becomes visible. Overlined frequencies correspond to scaled values using scaling factors of 0.9604 (normal) and 0.9572 (local frequencies) obtained with the experimental frequencies of $Ni(CO)_4$. Electron density, ρ_σ, and energy density, H_σ, were calculated at the bond critical point $\mathbf{r}_c(CO)$. For a numbering of complexes, see Figure 8. M06/aug-cc-pVTZ calculations. [b]M06/aug-cc-pVTZ with effective core potential for the iodine atom. [c]M06/6-311G(d,p) had to be used to enforce convergence.
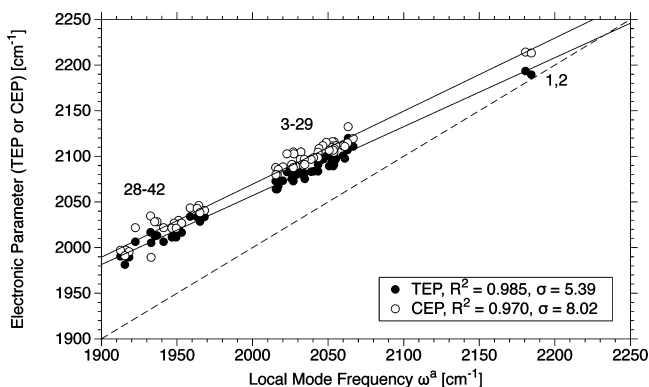
Figure 10. Comparison of LTEPw values with CEPs and TEPs for $LNi(CO)_3$ complexes **L1−L42**. Complexes with anionic ligands L are found in the low frequency part, with neutral L in the middle, and with cationic L in the high frequency part.
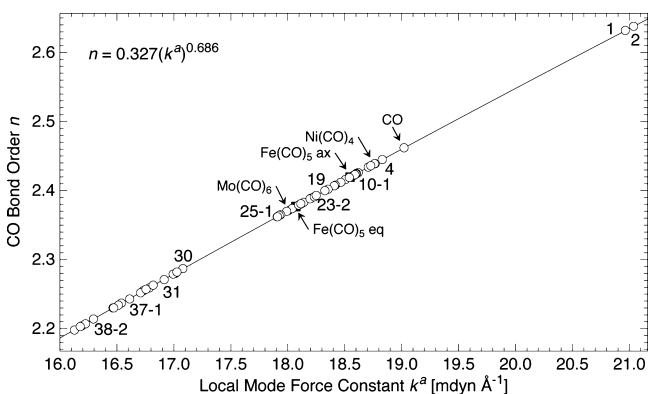
Figure 11. CO bond orders n given for **1, 2, 3**, free CO, and the $LNiCO_3$ complexes **L1−L42** as a function of the local CO stretching force constants, k^a.

In Figure 13a, the local NiL and NiC stretching force constants of $LNi(CO)_3$ (L = F⁻, Cl⁻, Br⁻, I⁻) are plotted as a function of the local CO stretching force constants. The inset of Figure 13a gives the relationship between $k^a(NiL)$ and $k^a(NiC)$. There exist (inverse) quadratic relationships in the latter two cases so that an inverse linear relationship between the NiL and CO bond strength (expressed by the local stretching force constants k^a) results confirming that a strong Ni−halogen bond leads to a larger charge transfer to Ni, stronger back-donation into the $\pi^\star(CO)$ orbital, and a subsequent decrease of the CO bond strength. Hence, the TEP is quantitatively justified, which, in view of the interaction mechanism discussed above, is reasonable.

In Figure 13b, the situation is analyzed for the phosphine ligands investigated in this work. Tolman's original work[1,2] focused on $R_3PNi(CO)_3$; therefore, this analysis is relevant. Although there is a linear relationship ($R^2 = 0.973$) between $k^a(CO)$ and $k^a(NiC)$, a similar relationship between $k^a(CO)$ and $k^a(NiP)$ does not exist. The analysis of the data reveals that
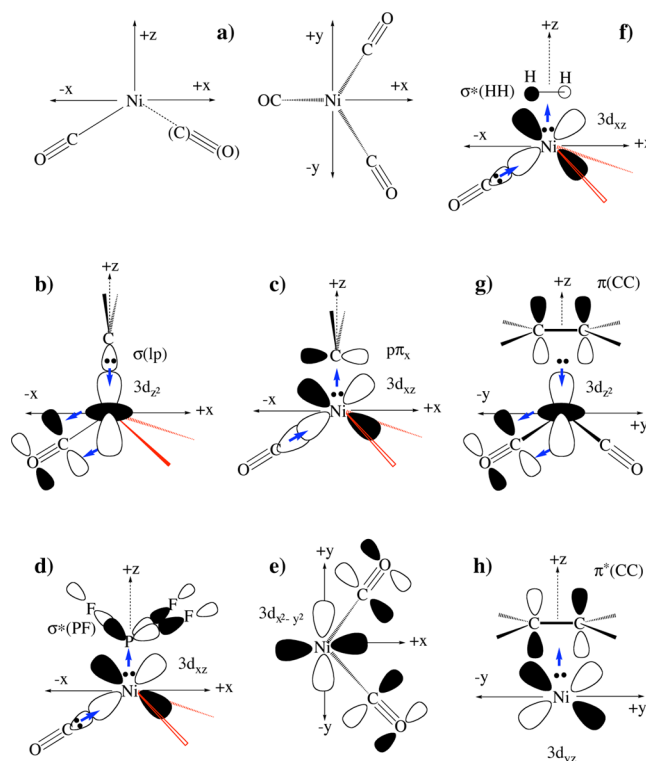

Figure 12. Orbital interaction diagrams between ligand L and the $Ni(CO)_3$ rest. (a) Coordinate system used. Atoms in parentheses are above or below the given plane. (b) σ-Donation from the lone-pair orbital of a carbene to the $3d_{z^2}(Ni)$ orbital followed by π-back-donation to the $\pi^\star(CO)$ orbitals. (c) Electron withdrawal from the $3d_{xz}(Ni)$ orbital into a $2p_x\pi$ orbital of a carbene leads to stronger σ-donation from the ip CO. (d) Electron withdrawal from the $3d_{xz}(Ni)$ orbital into the $\sigma^\star(PF)$ orbitals of PF_3 leads to stronger σ donation from the ip CO. (e) π-Back-donation from the $3d_{x^2+y^2}(Ni)$ orbital into the $\pi^\star(CO)$ orbitals of the oop CO ligands. (f) Electron withdrawal from the $3d_{xz}(Ni)$ orbital into the $\sigma^\star$ orbital of H_2 leads to stronger σ-donation from the ip CO. (g) Electron donation from the $\pi(CC)$ orbital of ethene into the $3d_{z^2}(Ni)$ orbital followed by π-back-donation to the $\pi^\star(CO)$ orbitals. (h) Electron withdrawal from the $3d_{yz}(Ni)$ orbital into the $\pi^\star(CC)$ orbital of ethene leads to stronger σ-donation from the oop CO ligands.

different situations can be distinguished. For L = PH_3, $PMeH_2$, and PMe_3, stronger phosphine−Ni bonding with increased hyperconjugative activation of the lone pair of P leads to an increase of electron density at Ni and back-donation to the $\pi^\star(CO)$ orbital. An inverse relationship between $k^a(NiL)$ and $k^a(CO)$ also obtained for the halogen ligands is suggested by the dashed line in Figure 13b.

For L = PH_3, PFH_2, PF_3, an increase rather than a decrease of the CO bond strength with an increase of the Ni−P bond strength is observed. This results from the fact that π-back-donation into the $\sigma^\star(PF)$ orbitals (see section 4) leads to a strengthening of the NiP bond but reduces also π-back-donation to CO. Hence, the basic assumption of the TEP that
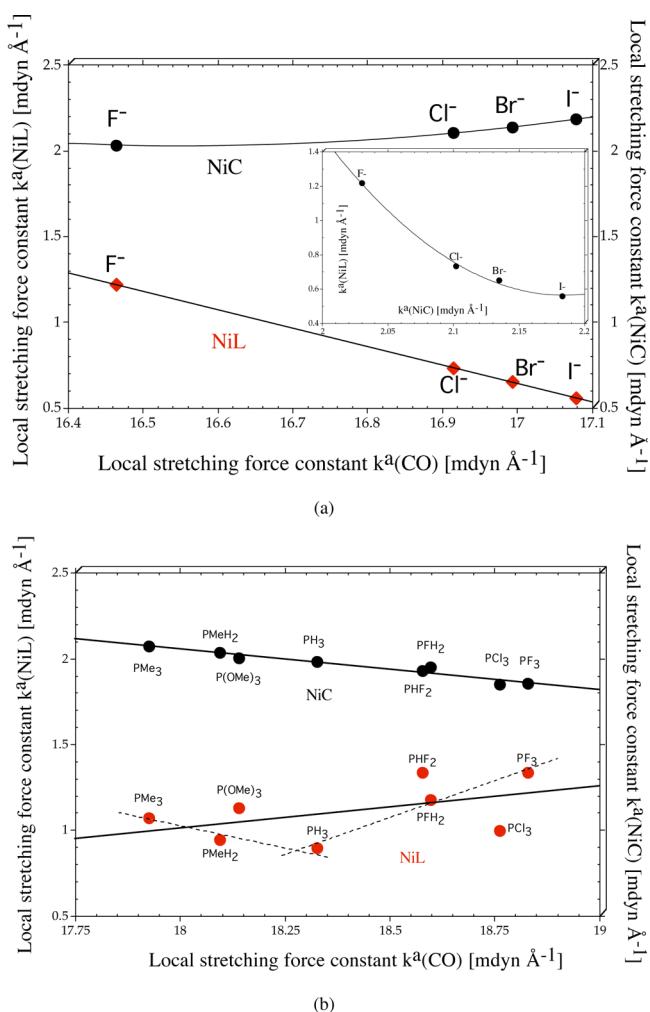
(a)

(b)

Figure 13. (a) Comparison of the local stretching force constants $k^a(CO)$ with the corresponding $k^a(NiL)$ and $k^a(NiC)$ values for complexes $LNi(CO)_3$ with $L = F^-, Cl^- Br^- I^-$. The inset gives a comparison between $k^a(NiC)$ and $k^a(NiL)$. (b) Comparison of the local stretching force constants $k^a(CO)$ with the corresponding $k^a(NiL)$ and $\bar{k}^a(NiC)$ values for complexes $LNi(CO)_3$ with $L =$ phosphine.

the strengthening of the Ni−L bond leads to an increase of the electron density at Ni is not fulfilled because of different Ni−L bonding mechanisms.

The situation becomes even more complicated in the case of symmetry lowering as for $L = PFH_2$, PHF_2 where different CO ligands have to be considered, steric effects as for $L = P(OMe)_3$, which lower the Ni−L bond strength, or for $L = PCl_3$, where the lower electronegativity of Cl changes the availability of the $\sigma^\star(PX)$ orbital and increases the availability of the P lone pair orbital for stronger electron donation to the Ni atom. Hence, the basic assumption of the TEP is no longer fulfilled and there is only a qualitative relationship between the strength of the Ni−L and CO bonds.

Because different electronic effects of L will affect the CO bond strength differently, the reliability of the TEP as an indirect NiL descriptor has to be investigated for each L. In any case, the local mode approach provides a direct measure for the M−L bond strength irrespective of the nature of M or L and provides for the first time insight into the quantitative or qualitative nature of the TEP. For ligands with similar electronic nature, e.g., $L = F^-, Cl^-, Br^-, I^-$, quantitative

relationships can be established and directly used in connection with the TEP.

6. CONCLUSIONS

This work has demonstrated that vibrational spectroscopy provides excellent tools to describe the electronic structure and chemical bonding in transition metal complexes. There are not many molecular properties that can be measured with a similar accuracy and, in addition, sensitively register small variations in the bonding structure of closely related molecules. Contrary to previous investigations of the TEP, we base our work on mode-decoupled local modes, which, via their properties, reliably describe the CO bond strength. Although mode coupling is relatively small (coupling frequencies up to 70 cm^{-1}), it leads to an erroneous order of TEP or CEP values. Clearly, Tolman could not refer to local modes when he started his work. Therefore, we see our work as an important extension of Tolman's seminal work.

(1) We have introduced the local mode-based electronic parameter LTEPw, which via the local CO stretching frequencies provides a direct measure of the CO bond strength without being flawed by mode coupling. LTEPw values have to be complemented by LTEPk (based on the local stretching force constant k^a) or the simpler to use LTEPn values (based on the CO bond order derived from k^a-constants) because the latter are no longer mass-dependent. The three parameters provide a reliable and unique description of the changes in the CO bond strength in dependence of changes with regard to the metal or the ligand sphere.

(2) The shortcomings of CEP and TEP values are caused by coupling of the CO stretching mode with metal−carbon stretching vibrations. The coupling frequencies quantify mode coupling and reveal significant errors if the highest a-symmetrical CO stretching frequency ω_μ is used. Depending on the complex symmetry and the mode coupling scheme different reduced masses are involved, which influences the TEP or CEP values significantly.

(3) An advantage of the LTEP concept is that its three parameters can be easily derived from either experimental or calculated frequencies (LCEP) where in the former cases just an auxiliary calculation based on perturbation theory is needed to obtain the force constant matrix associated with the experimental frequencies.

(4) There are significant differences between the TEP (or CEP) and the LTEP when describing the electronic properties of ligands L in $LNi(CO)_3$ complexes with regard to their magnitude or the relative electronic activity of closely related ligands L. Typical for such cases are the different orderings of carbenes, halogen anions, or chalcogen containing ligands.

(5) The analysis of the LTEP values reveals that one has to distinguish between σ and π effects of L, which lead to changes in the NiC and CO bond strengths. By using the LTEP values plus the local stretching force constants of all Ni bonds these effects can be separated. Depending on the orientation of a π-donor orbital of L, weakening or strengthening of the NiC bonds can be observed, which is especially relevant for carbene ligands and η-bonded ligands.

(6) The order of ligands based on the LTEP values can be fully rationalized by orbital interaction explanations based on PMO theory.

(7) With the LTEP values, electronic effects can be position-specifically identified, which is useful for complexes of lower symmetry, e.g., C_s-symmetry, as investigated in this work. It can

be concluded that LTEP values will also handle cases of strong steric interactions simplifying Tolman's use of two parameters (electronic and steric) to just one.

(8) The comparison of the homoleptic complexes $Ni(CO)_4$ (**1**), $Fe(CO)_5$ (**2**), and $Mo(CO)_6$ (**3**) reveals that LTEPs can be used to describe the electronic influence of the transition metal or that of the ligand sphere caused by their number or the overall arrangement. For example, the LTEP values provide a unique distiction between axial and equatorial CO groups in the case of **2**.

(9) Because the local mode approach presented in this work leads to a direct evaluation of the Ni-L bond strength via the local Ni-L bond stretching force constant, the use of the TEP as quantitative or qualitative descriptor of the Ni-L bond strength can be specified, which is discussed for two examples.

In future work, we will investigate how the LTEP approach presented in this work can be extended to transition metal complexes in general by utilizing local M−L stretching force constants directly.

■ ASSOCIATED CONTENT

Ⓢ Supporting Information

Decomposition tables, bond order plots, calculated electronic parameter (CEP) plots, C−O and Ni−X local mode force constants, geometries and NBO charges of **L1**−**L42**, adiabatic connection schemes (ACS) of CO frequency region, decompostion plots, and Cartesian coordinates. This material is available free of charge via the Internet at http://pubs.acs.org.

■ AUTHOR INFORMATION

Corresponding Author

*D. Cremer. E-mail: dieter.cremer@gmail.com.

Notes

The authors declare no competing financial interest.

■ ACKNOWLEDGMENTS

■ REFERENCES

(1) Tolman, C. A. *J. Am. Chem. Soc.* **1970**, *92*, 2953−2956.

(2) Tolman, C. A. *Chem. Rev.* **1977**, *77*, 313−348.

(3) Crabtree, *The Organometallic Chemistry of the Transition Metals*; Wiley, New York, 2009.

(4) Strohmeier, W.; Guttenberger, J. *Chem. Ber.* **1964**, *97*, 1871.

(5) Strohmeier, W.; Müller, F. *Z. Naturforsch., B: Anorg. Chem., Org. Chem., Biochem., Biophys., Biol.* **1967**, *22B*, 451.

(6) Horrocks, W. D., Jr.; Taylor, R. C. *Inorg. Chem.* **1963**, *2*, 723.

(7) Magee, T. A.; Matthews, C. N.; Wang, T. S.; Wotiz, J. *J. Am. Chem. Soc.* **1961**, *83*, 3200.

(8) Bond, A.; Carr, S.; Colton, R. *Organometallics* **1984**, *3*, 541.

(9) Grim, S.; Wheatland, D.; McFarlane, W. *J. Am. Chem. Soc.* **1967**, *89*, 5573.

(10) Cotton, F. A. *Inorg. Chem.* **1964**, *3*, 702−711.

(11) Alyea, E.; Ferguson, G.; Somogyvari, A. *Organometallics* **1983**, *2*, 668.

(12) Dalton, J.; Paul, I.; Smith, J. G.; Stone, F. A. *Chem. Soc. A* **1968**, 1195.

(13) Brown, R.; Dobson, G. *Inorg. Chim. Acta* **1972**, *6*, 65.

(14) Woodard, S.; Angelici, R.; Dombek, B. *Inorg. Chem.* **1978**, *17*, 1634.

(15) Angelici, R.; Sister, M.; Malone, B. *Inorg. Chem.* **1967**, *6*, 1731.

(16) Bancroft, M.; Dignard-Bailey, L.; Puddephatt, R. *Inorg. Chem.* **1986**, *25*, 3675.

(17) Darensbourg, D.; Nelson, H., III; Hyde, C. *Inorg. Chem.* **1974**, *13*, 2135.

(18) Cunningham, D.; Goldschmidt, Z.; Gottlieb, H.; Hezroni-Langerman, D. *Inorg. Chem.* **1991**, *30*, 4683.

(19) Inoue, H.; Nakagoma, T.; Kuroiwa, T.; Shirai, T.; Fluck, E. *Z. Naturforsch., B: J. Chem. Sci.* **1987**, *42B*, 573.

(20) Smith, R.; Baird, M. *Inorg. Chim. Acta* **1982**, *62*, 135.

(21) Howard, J.; Lovatt, J.; McArdle, P.; Cunningham, D.; Maimone, E.; Gottlieb, H.; Goldschmidt, Z. *Inorg. Chem. Commun.* **1998**, *1*, 118.

(22) Otto, S.; Roodt, A. *Inorg. Chim. Acta* **2004**, *357*, 1.

(23) Serron, S.; Huang, J.; Nolan, S. *Organometallics* **1998**, *17*, 534.

(24) Roodt, A.; Otto, S.; Steyl, G. *Coord. Chem. Rev.* **2003**, *245*, 121.

(25) Fürstner, A.; Alcarazo, M.; Krause, H.; Lehmann, C. W. *J. Am. Chem. Soc.* **2007**, *129*, 12676−12677.

(26) Canac, Y.; Lepetit, C.; Abdalilah, M.; Duhayon, C.; Chauvin, R. *J. Am. Chem. Soc.* **2008**, *130*, 8406−8413.

(27) Perrin, L.; Clot, E.; Eisenstein, O.; Loch, J.; Crabtree, R. H. *Inorg. Chem.* **2001**, *40*, 5806−5811.

(28) Gusev, D. G. *Organometallics* **2009**, *28*, 763−770.

(29) Gusev, D. G. *Organometallics* **2009**, *28*, 6458−6461.

(30) Tonner, R.; Frenking, G. *Organometallics* **2009**, *28*, 3901.

(31) Zobi, F. *Inorg. Chem.* **2009**, *48*, 10845−10855.

(32) Fianchini, M.; Cundari, T. R.; DeYonker, N. J.; Dias, H. V. R. *Dalton Trans.* **2009**, 2085.

(33) Fey, N.; Orpen, A. G.; Harvey, J. N. *Coord. Chem. Rev.* **2009**, *253*, 704−722.

(34) Fey, N. *Dalton Trans.* **2010**, *39*, 296−310.

(35) Kühl, O. *Coord. Chem. Rev.* **2005**, *249*, 693−704.

(36) Gillespie, A.; Pittard, K.; Cundari, T.; White, D. *Internet Electron. J. Mol. Des.* **2002**, *1*, 242−251.

(37) Cooney, K. D.; Cundari, T. R.; Hoffman, N. W.; Pittard, K. A.; Temple, M. D.; Zhao, Y. *J. Am. Chem. Soc.* **2003**, *125*, 4318−4324.

(38) Zeinalipour-Yazdi, C. D.; Cooksy, A. L.; Efstathiou, A. M. *Surf. Sci.* **2008**, *602*, 1858−1862.

(39) Kraihanzel, C. S.; Cotton, F. A. *Inorg. Chem.* **1963**, *2*, 533−540.

(40) Willner, H.; Schaebs, J.; Hwang, G.; Mistry, F.; Jones, R.; Trotter, J.; Aubke, F. *J. Am. Chem. Soc.* **1992**, *114*, 8972−8980.

(41) Zobi, F. *Inorg. Chem.* **2010**, *49*, 10370−10377.

(42) Suresh, C.; Koga, N. *Inorg. Chem.* **2002**, *41*, 1573.

(43) Giering, W.; Prock, A.; Fernandez, A. *Inorg. Chem.* **2003**, *42*, 8033.

(44) Park, E. S.; Boxer, S. G. *J. Phys. Chem. B* **2002**, *106*, 5800−5806.

(45) Alyea, E.; Song, S. *Comments Inorg. Chem.* **1996**, *18*, 189−221.

(46) Giering, W.; Prock, A.; Fernandez, A. *Inorg. Chem.* **2003**, *42*, 8033.

(47) Konkoli, Z.; Cremer, D. *Int. J. Quantum Chem.* **1998**, *67*, 1.

(48) Zou, W.; Kalescky, R.; Kraka, E.; Cremer, D. *J. Chem. Phys.* **2012**, *137*, 084114.

(49) Zou, W.; Kalescky, R.; Kraka, E.; Cremer, D. *J. Mol. Model.* **2012**, 1−13.

(50) Cremer, D.; Larsson, J. A.; Kraka, E. In *Theoretical Organic Chemistry*; Párkányi, C., Ed.; Theoretical and Computational Chemistry, Vol. *5*; Elsevier: Amsterdam, 1998; p 259.

(51) Kraka, E.; Larsson, J. A.; Cremer, D. In *Computational Spectroscopy: Methods, Experiments and Applications*; Grunenberg, J., Ed.; Wiley: New York, 2010; p 105.

(52) Kalescky, R.; Kraka, E.; Cremer, D. *J. Phys. Chem. A* **2013**, *117*, 8981−8995.

(53) Kraka, E.; Cremer, D. *ChemPhysChem* **2009**, *10*, 686.

(54) Wilson, E. B.; Decius, J. C.; Cross, P. C. *Molecular Vibrations. The Theory of Infrared and Raman Vibrational Spectra*; McGraw-Hill: New York, 1955.

(55) Rauhut, G.; Pulay, P. *J. Phys. Chem.* **1995**, *99*, 3093−3100.

(56) Merrick, J. P.; Moran, D.; Radom, L. *J. Phys. Chem. A* **2007**, *111*, 11683−11700.

(57) Kalescky, R.; Zou, W.; Kraka, E.; Cremer, D. *Chem. Phys. Lett.* **2012**, *554*, 243−247.

494

dx.doi.org/10.1021/ic4024663 | *Inorg. Chem.* 2014, 53, 478−495

(58) Kalescky, R.; Kraka, E.; Cremer, D. *Mol. Phys.* **2013**, *111*, 1497−1510.

(59) Freindorf, M.; Kraka, E.; Cremer, D. *Int. J. Quantum Chem.* **2012**, *112*, 3174−3187.

(60) Badger, R. M. *J. Chem. Phys.* **1934**, *2*, 128.

(61) Shimanouchi, T. *Tables of Molecular Vibrational Frequencies Consolidated*, Vol. *1*; National Bureau of Standards: Washington, DC, 1972.

(62) Becke, A. D. *J. Chem. Phys.* **1993**, *98*, 5648.

(63) Stevens, P. J.; Devlin, F. J.; Chablowski, C. F.; Frisch, M. J. *J. Phys. Chem.* **1994**, *98*, 11623.

(64) Truhlar, D. G. *Theor. Chem. Acc.* **2008**, *120*, 215Ð241.

(65) Dunning, T. H. *J. Chem. Phys.* **1989**, *90*, 1007.

(66) Kendall, R.; Dunning, T., Jr; Harrison, R. J. *J. Chem. Phys.* **1992**, *96*, 6796−6806.

(67) Konkoli, Z.; Cremer, D. *Int. J. Quantum Chem.* **1998**, *67*, 29.

(68) Kraka, E.; Filatov, M.; Zou, W.; Gräfenstein, J.; Joo, H.; Izotov, D.; Gauss, J.; He, Y.; Wu, A.; Polo, V.; Olsson, L.; Konkoli, Z.; He, Z.; Cremer, D. *COLOGNE2013*; Southern Methodist University: Dallas, TX, 2013.

(69) Jones, L. H. *J. Chem. Phys.* **1958**, *28*, 1215.

(70) Cormier, A. D.; Brown, J. D.; Nakamoto, K. *Inorg. Chem.* **1973**, *12*, 3011−3013.

(71) Edgell, W. F.; Wilson, W. E.; Summitt, R. *Spectrochim. Acta* **1963**, *19*, 863−872.

(72) Jones, L. H.; McDowell, R. S.; Goldblatt, M. *Inorg. Chem.* **1969**, *8*, 2349−2363.

(73) Hedberg, L.; Iijima, T.; Hedberg, K. *J. Chem. Phys.* **1979**, *70*, 3224.

(74) Braga, D.; Grepioni, F.; Orpen, A. *Organometallics* **1993**, *12*, 1481.

(75) Luo, Y.-R. *Comprehensive Handbook of Chemical Bond Energies*; Taylor and Francis: Boca Raton, FL, 2007.

(76) Beagley, B.; Schmidling, D. G. *J. Mol. Struct.* **1974**, *22*, 466.

(77) Jonas, V.; Thiel, W. *J. Chem. Phys.* **1995**, *102*, 8474−8484.

(78) Jang, J. H.; Lee, J. G.; Lee, H.; Xie, Y.; Schaefer, H. F., III *J. Phys. Chem. A* **1998**, *102*, 5298−5304.

(79) Porterfield, W. W. *Inorganic Chemistry, A Unified Approach*; Academic Press: San Diego, 1993.

(80) Arnesen, S.; Selp, H. M. *Acta Chem. Scand.* **1966**, *20*, 2711.

(81) Mak, T. C. W. *Z. Kristallogr.* **1984**, *166*, 277.

(82) Cremer, D.; Kraka, E. *Croat. Chem. Acta* **1984**, *57*, 1259.

(83) Cremer, D.; Kraka, E. *Angew. Chem., Int. Edt.* **1984**, *23*, 627.

(84) Haynes, W. M., Ed. *Handbook of Chemistry and Physics*, 92nd ed.; CRC PRESS: Boca Raton, FL, 2011.